Chapter 3. Elastic Scattering and Optical Model

Contents

1 Classical scattering

1.1 Useful units in the nuclear reactions

Quantities	Unit
Energy	MeV
mass	MeV/c^2
Wave number	fm^{-1}
Atomic mass unit	931.494 MeV
m_p	938.272 MeV
m_n	939.573 MeV
m_e	0.511 MeV
$\hbar c$	197.337 MeV ·fm
$\alpha = e^2/\hbar c$	137.036^{-1}
Wave number unit	$0.219\sqrt{AE}$ fm^{-1}
	$k = \sqrt{2 \times amuAE}/\hbar c$
	A = mass number
Relative velocity	$4.633 \times 10^{-2}\sqrt{E_{lab}/A_P}$
	$v/c = \sqrt{2E_{lab}/m_P}$
	A_P Proj. mass #
Sommerfeld parameter unit	$7.298 \times 10^{-3} Z_P Z_T (c/v)$
	$\eta = (e^2/\hbar c) Z_P Z_T (c/v)$
	$Z_P(Z_T)$ Proj(target) charge
η/k	$Z_P Z_T/(1.389E)$

1.2 Classical (non-relativistic) kinematics

In the Lab system, the target (m_T) is at rest, while projectile (m_P) is moving with velocity v_P, then

$$\begin{aligned}
\text{position vector of projectile :} \quad & \vec{r}_P \\
\text{position vector of target :} \quad & \vec{r}_T \\
\text{position vector of c.m. point :} \quad & \vec{R} = \frac{m_P\vec{r}_P + m_T\vec{r}_T}{m_P + m_T} \\
\text{velocity vector of projectile :} \quad & \vec{v}_P \\
\text{velocity vector of target :} \quad & 0 \\
\text{velocity vector of c.m. point :} \quad & \vec{V} = \frac{m_P\vec{v}_P}{m_P + m_T} \\
\text{total velocity vector of lab system :} \quad & \vec{V}_L = \vec{V} = \frac{m_P\vec{v}_P}{m_P + m_T} \\
& = \frac{\vec{p}_L}{m_P + m_T}
\end{aligned}$$

where $\vec{p}_L$ is the momentum of the projectile.

The center of mass (c.m.) system is defined as,

$$\begin{aligned}
\text{total velocity vector of c.m. system :} \quad & \vec{V} = 0 \\
& \vec{p}_P = -\vec{p}_T = \vec{p}
\end{aligned}$$

$\vec{p}$ is the common magnitude of $\vec{p}_P$ and $\vec{p}_T$ and has a direction of the projectile. The center of mass frame is moving to the right (projectile direction) with the velocity $\vec{V}_L$. Hence

$$\begin{aligned}
\vec{p}_L &= \vec{p} + m_P \vec{V}_L \\
\vec{p} &= \vec{p}_L - m_P \vec{V}_L = \frac{m_T}{m_P + m_T} \vec{p}_L \\
E_L &= \frac{\vec{p}_L^2}{2m_P} = \frac{\vec{p}^2 (m_P + m_T)^2}{2 m_P m_T^2} \\
E &= \frac{\vec{p}^2}{2m_P} + \frac{\vec{p}^2}{2m_T} = \frac{\vec{p}^2 (m_P + m_T)}{2 m_P m_T} \\
&= \frac{m_T}{(m_P + m_T)} E_L \\
&= \frac{\vec{p}^2}{2\mu} \\
\mu &= \frac{m_P m_T}{(m_P + m_T)} \quad \text{Reduced mass.}
\end{aligned}$$

The energy of the c. m. point in the lab frame,

$$E' = \frac{1}{2}(m_P + m_T) V_L^2 = \frac{m_P}{(m_P + m_T)} E_L$$

remains constant and is thus not available for the reaction. Of course, $E + E_{cm} = E_L$.

1.3 Relativistic kinematics

What we want to do is the Lorentz transformation of Lab system to c.m. system such that, in the natural unit system ($\hbar = c = 1$)

$$(E_0 + m_T, k_0) \quad \rightarrow \quad (\omega, 0)$$

where $E_0 - m_P = E_{lab}$, and $E_0^2 = m_P^2 + k_0^2$. Note that E_{lab} denotes the kinetic energy of lab system. Thus we have

$$\begin{aligned}
\begin{pmatrix} \omega \\ 0 \end{pmatrix} &= \begin{pmatrix} \gamma & -\gamma\beta \\ -\gamma\beta & \gamma \end{pmatrix} \begin{pmatrix} E_0 + m_T \\ k_0 \end{pmatrix} \\
\beta_{cm} &= \frac{\vec{k}_0}{E_0 + m_T} \quad \text{(Velocity of c.m. wrt lab frame)} \\
\gamma_{cm} &= \frac{1}{\sqrt{1 - \beta^2}} = \frac{E_0 + m_T}{\sqrt{(E_0 + m_T)^2 - k_0^2}} \\
&= \frac{E_0 + m_T}{\sqrt{s}} \\
s &= \omega^2 = (E_0 + m_T)^2 - k_0^2 \\
&= (E_{lab} + m_P + m_T)^2 - (E_{lab} + m_P)^2 + m_P^2 \\
&= (m_P + m_T)^2 + 2 E_{lab} m_T
\end{aligned}$$

Thus the c.m. kinetic energy, E_{cm}, is simply

$$E_{cm} = \omega - (m_T + m_P) = \sqrt{s} - (m_T + m_P)$$

We now obtain the c.m. energy and wave numbers by Lorentz transformation of (E_0, k_0),

$$\begin{aligned}
\begin{pmatrix} E \\ k \end{pmatrix} &= \begin{pmatrix} \gamma & -\gamma\beta \\ -\gamma\beta & \gamma \end{pmatrix} \begin{pmatrix} E_0 \\ k_0 \end{pmatrix} \\
&= \frac{1}{\sqrt{s}} \begin{pmatrix} s - m_T^2 - m_T E_0 \\ m_T k_0 \end{pmatrix}
\end{aligned}$$

since

$$\begin{aligned} E &= \gamma E_0 - \gamma\beta k_0 = \frac{E_0+m_T}{\sqrt{s}}(E_0 - \frac{k_0^2}{E_0+m_T}) \\ &= \frac{1}{\sqrt{s}}[(E_0+m_T)^2 - k_0^2 - m_T E_0 - m_T^2] \\ &= \frac{1}{\sqrt{s}}(s - m_T^2 - m_T E_0) \\ k_{cm} &= -\gamma\beta E_0 + \gamma k_0 = \frac{E_0+m_T}{\sqrt{s}}(-\frac{E_0 k_0}{E_0+m_T} + k_0) \\ &= \frac{1}{\sqrt{s}} m_T k_0 \end{aligned}$$

We thus have the wave number and the masses of target and projectile in the c.m. system, as follows.

$$\begin{aligned} k_{cm}^2 &= \frac{m_T^2}{s}k_0^2 = \frac{m_T^2}{s}(E_0^2 - m_P^2) \\ &= \frac{m_T^2}{s}[(E_{lab}+m_P^2)^2 - m_P^2] \\ &= \frac{m_T^2}{s}(E_{lab}^2 + 2E_{lab}m_P) \\ m_T' &= \gamma_{cm} m_T = \frac{E_0+m_T}{\sqrt{s}} \\ &= \frac{m_T}{\sqrt{s}}(E_{lab} + m_P + m_T) \\ m_P' &= (1+\beta_0\beta_{cm})\gamma_0\gamma_{cm} m_P \text{ with } \beta_0 = \frac{k_0}{E_0},\ \gamma_0 = \frac{E_0}{m_P} \\ &= [1 + \frac{k_0^2}{E_0(E_0+m_T)}]\frac{E_0(E_0+m_T)}{\sqrt{s}} \\ &= \frac{1}{\sqrt{s}}[E_0^2 + E_0 m_T + k_0^2] \\ &= \frac{1}{\sqrt{s}}[2E_0^2 + E_0 m_T - m_P^2] \\ &= \frac{1}{\sqrt{s}}[2E_{lab}^2 + 4E_{lab}m_P + m_P(m_P+m_T) \\ &\quad + E_{lab}m_T] \\ &\approx \frac{1}{\sqrt{s}}[m_P(m_P+m_T) + E_{lab}m_T] \end{aligned}$$

with $m_T >> m_P$ or E_{lab}.

Homework #6: 1. Draw E_{lab} in MeV vs. wavelength λ in fm for electron, proton, ^{16}O, and ^{208}Pb on ^{208}Pb using the non-relativistic and relativistic kinematics. Discuss physics.

1.4 Scattering in the central force field

[For this subsection, refer "Classical Mechanics, Section 3-11" by H. Goldstein.]

1.4.1 Differential cross section

The cross section for scattering in a given direction, $\sigma(\Omega)$, is defined by

$$\sigma(\Omega) = \frac{\#\text{ of particles scattered into } d\Omega \text{ per unit time}}{\text{incident intensity}}$$

The angular momentum ℓ can be expressed in term of the energy and the *impact parameter*, b, defined as the perpendicular distance between the center of force and the incident velocity. If v_0 is the incident speed of the particle, then

$$\ell = mv_0 b = b\sqrt{2mE}$$

The number of particles scattered into a solid angle $d\Omega$ lying between Θ and $\Theta + d\Theta$ must be equal to the number of the incident particles with impact parameter lying between the corresponding b and $b + db$:

$$2\pi I b|db| = 2\pi\sigma(\Theta) I \sin\Theta |d\Theta|.$$

where I is the intensity, i.e., the number of particles crossing unit area normal to the beam in unit time. If b is considered as a function of the energy and the corresponding scattering angle, then the dependence of the differential cross section on Θ is given by

$$\sigma(\Theta) = \frac{b}{\sin\Theta}\left|\frac{db}{d\Theta}\right|$$

1.4.2 Repulsive nonsingular potential

Consider a repulsive potential and particle energy shown in Fig. 3-21(a). It is easy to see physically that the curve of Θ versus b may behave as indicated in Fig. 3-21(b). Thus, with very large values of impact parameter, the particle always remains at the large radial distances from the center of force and suffers only minor deflection. At the other extreme, for $b = 0$, the particle travels in a straight line into the center of force, and if the energy is greater that the maximum of the potential, it will continue on through the center without being scattered at all. Hence, for both limits in b the scattering angle goes to zero. For some intermediate value of b the scattering angle must pass through a maximum Θ_m. When $\Theta < \Theta_m$ there will be two values of b that can give rise to the dame scattering angle. Each will contribute to the scattering cross section at that angle, and the cross section should accordingly be modified to the form

$$\sigma(\Theta) = \sum_i \frac{b_i}{\sin\Theta}\left|\frac{db}{d\Theta}\right|_i$$

Rainbow scattering: Of particular interest is the cross section at the maximum angle of scattering Θ_m. As the derivative of Θ with respect to s vanishes at this angle, it follows that the cross section must become infinite at $\Theta \to \Theta_m$. But for all larger angles the cross section is zero, since the scattering angle cannot exceed Θ_m. The phenomenon of the infinite rise of the cross section followed by abrupt disappearance is very similar to what occurs in the geometrical optics of the scattering of sunlight by raindrops. On the basis of this similarity the phenomenon is called *rainbow scattering*.

1.4.3 Attractive potential

Under the attractive potential, the effect of attraction will be to pull the particle in toward the center instead of the repulsive deflection outward, and the scattering angle can be negative. This in itself is no great difficulty as clearly it is the magnitude of Θ that is involved in finding the cross section. But, under certain circumstances Θ may be greater than 2π. That is the particle undergoing scattering may circle the center of force for one or more revolutions before going off finally in the scattered direction. Consider a scattering potential shown schematically

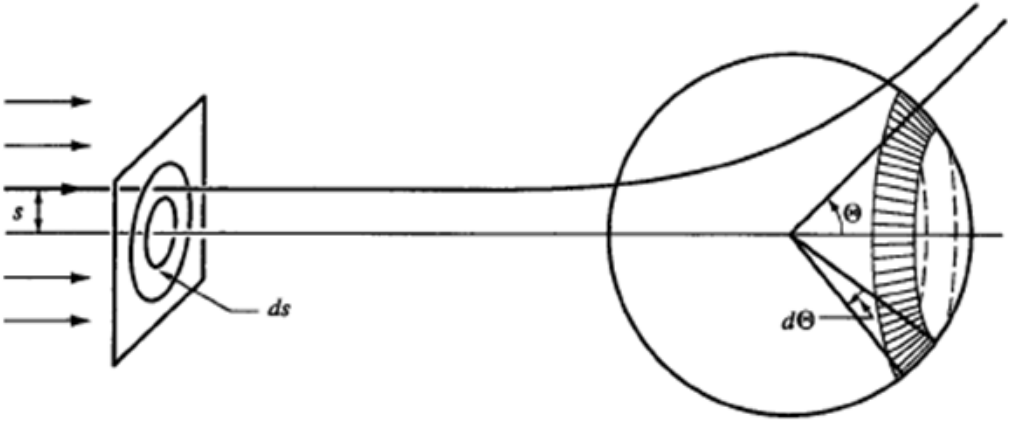

FIGURE 3.19 Scattering of an incident beam of particles by a center of force.

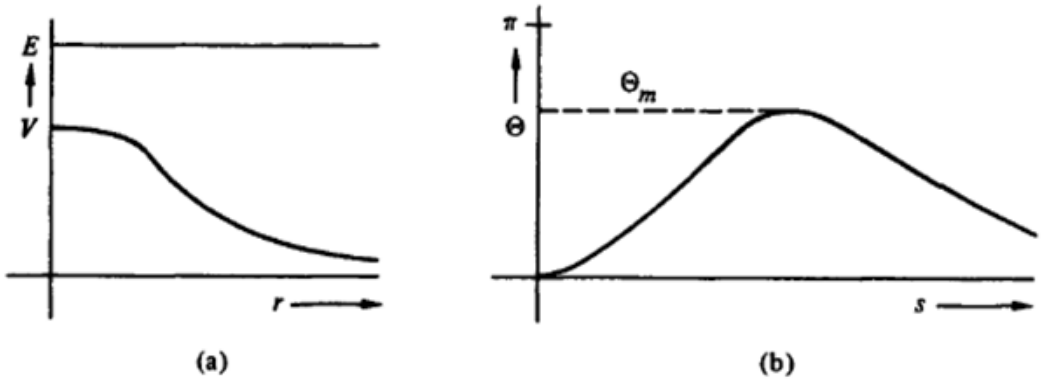

FIGURE 3.21 Repulsive nonsingular scattering potential and double-valued curve of scattering angle Θ versus impact parameter s_0 for sufficiently high energy.

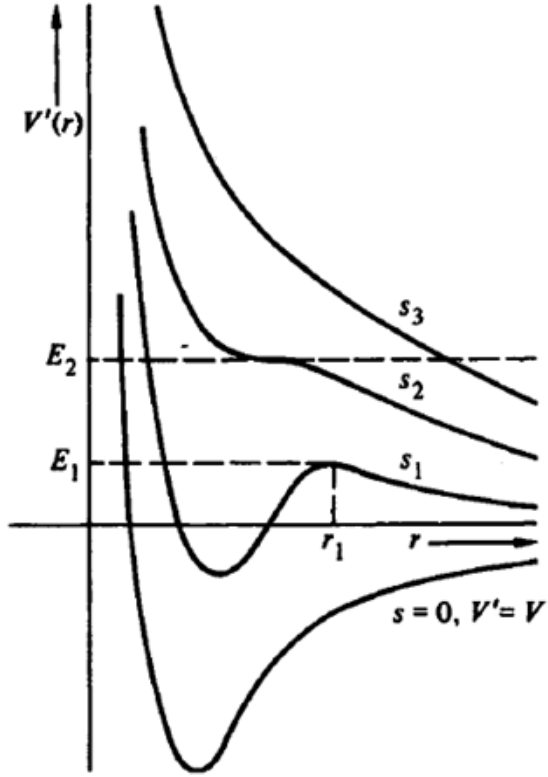

FIGURE 3.22 A combined attractive and repulsive scattering potential, and the corresponding equivalent one-dimensional potential at several values of the impact parameter s.

as the $b = 0$ curve in Fig. 3-22, like the NN interaction. The other curves in Fig. 3-22 show the effective potentials for the various values of the impact parameter.

Orbiting: Consider an incoming particle with impact parameter s_1 and at the energy E_1 corresponding to the maximum of the hump. When the incoming particle reaches r_1, the radial velocity is zero, which means that the particle would circle around the center of force indefinitely at that distance without ever emerging! In such instance the classical scattering is said to exhibit *orbiting* or *spiraling*.

Deflection angle: The scattered particle may then be deflected by more than π when orbiting takes place. On the other hand, the observed scattering angle in the lab lies between 0 and π. It is therefore helpful in such ambiguous cases to distinguish between a *deflection angle* Φ and the observed scattering angle Θ. For give Φ, the angle Θ is to be determined from the relation, $\Theta = \pm\Phi - 2m\pi$. The sign and the values of m are to be chosen so that Θ lies between 0 and π. Fig. 3-23 shows schematic curves of Φ versus b for the potential of Fig. 3-22 at two different energies. The orbiting that takes place for $E = E_1$ shows up as s singularity at $b = s_1$.

Glory scattering When $E > E_2$, orbiting no longer takes places but there is a rainbow effect at $\Theta = -\Phi'$. It will be noticed that Θ vanishes at $b = s_3$, which gives that the cross section becomes infinite in the forward direction through the vanishing of $\sin\Theta$. The cross section can similarly become infinite in the backward direction if $b|ds/d\Theta|$ remains finite at $\Theta = \pi$. Theses infinities are referred to as *glory scattering*.

1.5 Scattering in the center of mass frame

Let θ and Θ be the scattering angles in the center-of-mass (CM) frame in which the theories have been developed and in the lab frame of the experiment, respectively. we show that the scattering angle θ and Θ in the elastic scattering is related by

$$\tan\Theta = \frac{\sin\theta}{\alpha + \cos\theta}, \quad \alpha \equiv \frac{m_1}{m_2}$$

This is a classical mechanics problem. We sketch out from "Classical Mechanics, Section 3-11" by H. Goldstein.

Let $\mathbf{r}_1$ and $\mathbf{v}_1$ be the position and velocity, after scattering, of the incident particle 1 in the lab frame, $\mathbf{r'}_1$ and $\mathbf{v'}_1$ be the position and velocity, after scattering, of the incident particle 1 in the CM frame, and $\mathbf{R}$ and $\mathbf{V}$ be the position and velocity of the CM in the lab frame. We thus have

$$\mathbf{r}_1 = \mathbf{R} + \mathbf{r}'_1, \quad \mathbf{v}_1 = \mathbf{V} + \mathbf{v}'_1$$

After the scattering, $\mathbf{v}_1$ and $\mathbf{v'}_1$ make the angles Θ and θ, respectively, with the vector $\mathbf{V}$ lying along the initial direction. Since the target is initially stationary in the lab system, the incident velocity of particle 1 in the lab, $\mathbf{v}_0$ is the same as the initial velocity of the particles. Conservation of the total linear momentum gives

$$(m_1 + m_2)\mathbf{V} = m_1\mathbf{v}_0, \;\; \Rightarrow \;\; \mathbf{V} = \frac{\mu}{m_2}\mathbf{v}_0, \;\; \mu \equiv \frac{m_1 m_2}{m_1 + m_2}$$

The triangle with sides $\mathbf{v}_1, \mathbf{v}'_1$ and $\mathbf{V}(\parallel \mathbf{v}_0)$ gives relations

$$\begin{aligned} v_1 \sin\Theta &= v'_1 \sin\theta \\ v_1 \cos\Theta &= v'_1 \cos\theta + V \end{aligned}$$

We thus obtain

$$\tan\Theta = \frac{\sin\theta}{\beta + \cos\theta}, \quad \beta \equiv \frac{\mu}{m_2}\frac{v_0}{v'_1}$$

By the definition of v'_1, we have

$$v'_1 = \frac{\mu}{m_1} v$$

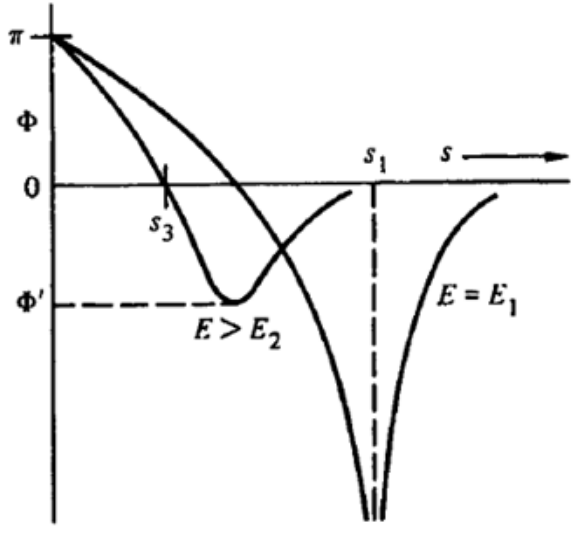

FIGURE 3.23 Curves of deflection angle Φ versus s, for the potential of Fig. 3.22 at two different energies.

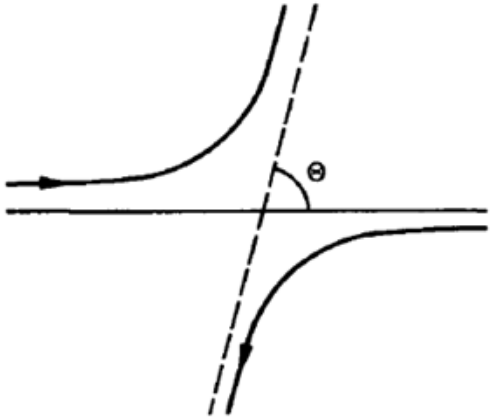

FIGURE 3.25 Scattering of two particles as viewed in the center of mass system.

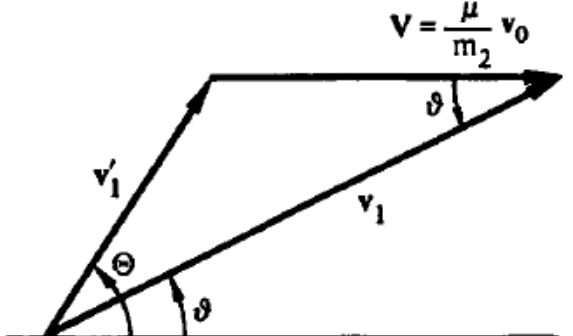

FIGURE 3.26 The relations between the velocities in the center of mass and laboratory coordinates.

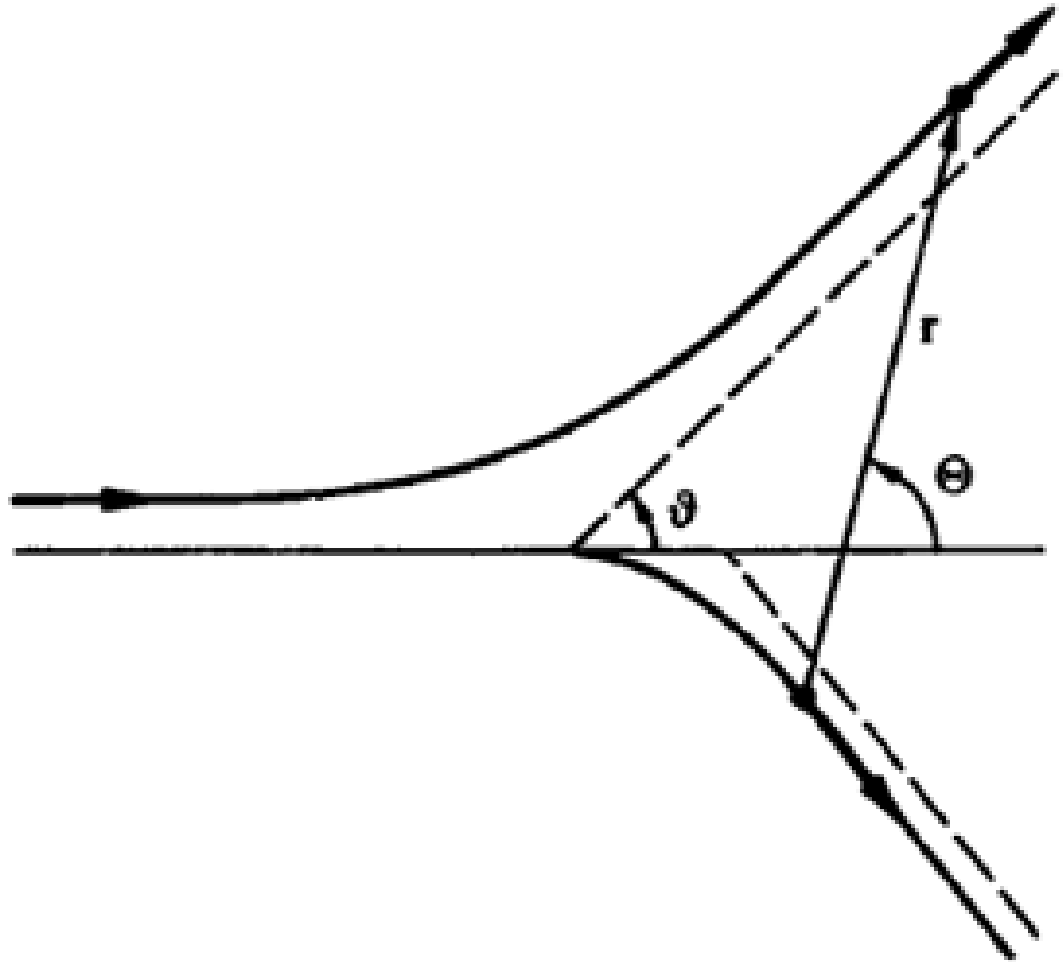

FIGURE 3.24 Scattering of two particles as viewed in the laboratory system.

where v is the relative speed after the scattering. For the elastic scattering $v = v_0$. It yields

$$\beta = \frac{\mu}{m_2}\frac{v_0}{v_1'} = \frac{\mu}{m_2}\frac{m_1 v_0}{\mu v} = \frac{m_1}{m_2} = \alpha$$

We finally obtain the desired result.

$$\tan\Theta = \frac{\sin\theta}{\alpha + \cos\theta}, \quad \alpha \equiv \frac{m_1}{m_2}$$

There are several comments;
(1) When $\alpha \ll 1,\ m_2 \gg m_1$, $\Theta \approx \theta$.
(2) When $\alpha = 1,\ m_2 = m_1$,

$$\tan\Theta = \frac{\sin\theta}{1 + \cos\theta} = \tan(\theta/2)$$

so that $\Theta = \theta/2$.

(3) When $\alpha > 1,\ m_2 < m_1$, the incident projectile can no longer scatter backwards in the lab frame, even for head-on collisions, the heavier particles proceed forward. There are two CM angles corresponding to a given lab angle.

Homework #6: 2. Draw Θ in deg vs. θ in deg for $\alpha = 0.0, 0.5, 0.9, 1.0, 1.1$ and 2.0. Discuss physics.

We next show that the scattering cross sections σ_C and σ_L is related by

$$\frac{d\sigma_L}{d\cos\Theta} = \frac{d\sigma_C}{d\cos\theta}\frac{(1 + \alpha^2 + 2\alpha\cos\theta)^{3/2}}{1 + \alpha\cos\theta}$$

A relation between the scattering cross sections σ_C and σ can be obtained from the fact that in a particular experiment the number of particles scattered into a given element of solid angle must be the same whether we measure the event in terms of θ or Θ, that is

$$\begin{aligned} J_{inc}(d\sigma_L/d\Omega_L)d\Omega_L &= J_{inc}(d\sigma_C/d\Omega_C)d\Omega_C \\ \frac{d\sigma_L}{d\cos\Theta} &= \frac{d\sigma_C}{d\cos\theta}\frac{d\cos\theta}{d\cos\Theta} \end{aligned}$$

Squaring the result of (a) gives

$$\begin{aligned} \frac{1}{\cos^2\Theta} - 1 &= \frac{1 - \cos^2\theta}{(\alpha + \cos\theta)^2} \\ \frac{1}{\cos^2\Theta} &= \frac{1 - \cos^2\theta + (\alpha + \cos\theta)^2}{(\alpha + \cos\theta)^2} \\ \cos\Theta &= \frac{\alpha + \cos\theta}{\sqrt{1 + 2\alpha\cos\theta + \alpha^2}} \end{aligned}$$

We now evaluate

$$\begin{aligned} \frac{d\cos\Theta}{d\cos\theta} &= \frac{1 + 2\alpha\cos\theta + \alpha^2 - (\alpha + \cos\theta)(2\alpha/2)}{(\sqrt{1 + 2\alpha\cos\theta + \alpha^2})^3} \\ &= \frac{1 + \alpha\cos\theta}{(\sqrt{1 + 2\alpha\cos\theta + \alpha^2})^3} \end{aligned}$$

We obtain

$$\frac{d\sigma_L}{d\cos\Theta} = \frac{d\sigma_C}{d\cos\theta}\frac{(1 + \alpha^2 + 2\alpha\cos\theta)^{3/2}}{1 + \alpha\cos\theta}$$

It implies that isotropic scattering in the CM is not isotropic in the lab system.

For the special case of equal-mass particles, where $\theta = 2\Theta$,

$$\begin{aligned} \frac{d\sigma_L}{d\cos\Theta} &= \frac{d\sigma_C}{d\cos\theta}\frac{(1+1+2\cos 2\Theta)^{3/2}}{1+\cos 2\Theta} \\ \frac{1}{4\cos\Theta}\frac{d\sigma_L}{d\cos\Theta} &= \frac{d\sigma_C}{d\cos\theta} \end{aligned}$$

since

$$\frac{(2+2\cos 2\Theta)^{3/2}}{1+\cos 2\Theta} = 2^{3/2}\sqrt{1+\cos 2\Theta} = 4\cos\Theta$$

1.6 Coulomb scattering

The classical Coulomb scattering trajectories of two colliding ions in the c.m. systems are the conic sections with a eccentricity $\epsilon > 1$,

$$\begin{aligned} \frac{1}{r} &= \frac{\mu Z_P Z_T e^2}{\ell^2}(1-\epsilon\cos\phi) \\ \epsilon^2 &= 1+\frac{2E\ell^2}{\mu Z_P^2 Z_T^2 e^4} \end{aligned}$$

With a boundary condition that $r \to \infty$, the scattering angle $\theta = \phi$, we have

$$\cos\phi = \frac{1}{\epsilon}$$

which means that for a given ℓ the trajectory is uniquely determined;

$$\begin{aligned} \tan\frac{\theta}{2} &= \tan(\frac{\pi}{2}-\phi) = \cot\phi \\ &= \frac{1}{\sqrt{\epsilon^2-1}} = \sqrt{\frac{\mu Z_P^2 Z_T^2 e^4}{2E\ell^2}} \\ \epsilon &= \csc\frac{\theta}{2} \end{aligned}$$

If we introduce the parameter a, defined as one-half the distance of closest approach in a head-on collision ($\theta = 180$)

$$a = \frac{Z_P Z_T e^2}{\mu v_0^2} = \frac{Z_P Z_T e^2}{2E}$$

then the factor $\frac{\mu Z_P Z_T e^2}{\ell^2}$ in the orbit equation becomes

$$\frac{\mu Z_P Z_T e^2}{\ell^2} \times a = \frac{\mu Z_P^2 Z_T^2 e^4}{2E\ell^2} = \frac{1}{\epsilon^2-1}$$

The orbit equation can be read as

$$r = \frac{a(\epsilon^2-1)}{1-\epsilon\cos\phi}$$

We further define the so-called *Sommerfeld parameter*, together with the asymptotic wavelength of relative motion at large separation, $\bar{\lambda} = \hbar/\mu v_0$,

$$\eta = \frac{a}{\bar{\lambda}} = \frac{Z_P Z_T e^2}{\hbar v_0} = ka$$

We now introduce the *impact parameter*, b, which would be closest approach for no force. The angular momentum becomes

$$\begin{aligned} \ell &= \mu v_0 b = \sqrt{2\mu E} b \\ b &= \frac{Z_P Z_T e^2}{2E} \cot\frac{\theta}{2} = \frac{\eta}{k}\cot\frac{\theta}{2} \end{aligned}$$

The famous Rutherford scattering cross section becomes

$$\begin{aligned} \sigma(\theta) &= \frac{b}{\sin\theta}\left|\frac{db}{d\theta}\right| \\ &= \frac{1}{4}\left(\frac{Z_P Z_T e^2}{2E}\right)^2 \csc^4\left(\frac{\theta}{2}\right) \end{aligned}$$

Finally, we define the parameter d, the distance of closest approach, which is widely used in heavy-ion physics. Setting $\cos\phi = 0$ in the orbit equation gives

$$d = a(1+\epsilon) = \frac{\eta}{k}\left(1 + \csc\frac{\theta}{2}\right)$$

The requirement of energy conservation from infinity to the point of closest approach (turning point) leads to

$$\begin{aligned} E &= \frac{Z_P Z_T e^2}{d} + \frac{\ell^2\hbar^2}{2\mu d^2} \\ \ell^2 &= \frac{2\mu E d^2}{\hbar^2} - 2dk\frac{Z_P Z_T e^2 \mu}{\hbar^2 k} \\ &= kd(kd - 2\eta) \\ kd &= \eta + \sqrt{\eta^2 + \ell^2} \\ \sin\frac{\theta}{2} &= \frac{\eta}{kd - \eta} = \frac{\eta}{\sqrt{\eta^2 + \ell^2}} \end{aligned}$$

These relationships are important in the semiclassical analysis of heavy-ion scattering. In practice, we use

$$\begin{aligned} a &= 0.720\frac{Z_P Z_T}{\mu_M e_{lab}} \quad \text{fm} \\ k &= 0.219\mu_M e_{lab}^{1/2} \quad \text{fm}^{-1} \\ \eta &= 0.158\frac{Z_P Z_T}{e_{lab}^{1/2}} \end{aligned}$$

where μ_M is the mass number of the reduced mass and e_{lab} is the lab energy per nucleon. Relationship between d, ℓ and θ can be summarized as

	Formula	in terms of	
	d	ℓ	θ
d	...	$a[1 + (1 + \ell^2/\eta^2)^{1/2}]$	$a[1 + \sin^{-1}(\theta/2)]$
ℓ	$\eta[d/a(d/a - 2)]^{1/2}$	...	$\eta\cot(\theta/2)$
θ	$2\sin^{-1}(a/(d-a))$	$2\tan^{-1}(\eta/\ell)$	...

1.7 Grazing collision

In the nuclear reactions, where repulsive Coulomb and short range attractive nuclear potentials exists, we have two different kinematic situations,

impact parameter	scattering angles	potential	trajectory
large	small	Coulomb	Coulomb
small	large	nuclear	inelastic

The interesting quantity is referred as the 'critical', 'glancing', 'peripheral', or *grazing* value,

$$R_{gr} = d$$

where d denotes the distance of closest approach. The grazing angle and grazing angular momentum are then, respectively,

$$\begin{aligned} \sin\frac{\theta_{gr}}{2} &= \frac{\eta}{kR_{gr}-\eta} = \frac{\eta}{\sqrt{\eta^2+\ell_{gr}^2}} \\ \ell_{gr}^2 &= kR_{gr}(kR_{gr}-2\eta) \end{aligned}$$

There is **no clear-cut value** of R_{gr} under the Coulomb and nuclear potentials.

1.8 Classical heavy-ion scattering

This subsection reviews the paper by N. K. Glendenning, *Rev. Mod. Phys.*, **47**, 659 (1975).

1) Effective interaction (Fig.1 of Glendenning)

2) Discontinuity in the distance of closest approach
(Penetration depth, or turning point)(Fig.2)

a) Coulomb orbit (Fig.3 and Fig.5)
b) Skimming orbit
c) plunging orbit
d) grazing orbit

3) Deflection function (Fig. 6)

$$\Theta(\ell) = \pi - 2b\int_{R_t}^{\infty} \frac{dr}{r^2\sqrt{1-V_{eff}/E_{cm}}}$$

4) Optical model analysis (Fig. 4)

Homework #6: 3. Consider the ^{18}O + ^{120}Sn system at $E_{lab} = 100$ MeV.

1) Draw $V_{eff}(r)$ in MeV vs. r in fm for $\ell = 0, 10, 20, 30,$
40, 50, 60, 70, 80, and 90.

$$\begin{aligned} V_{eff}(r) &= -\frac{40.0}{1+\exp[(r-1.31(A_T^{1/3}+A_P^{1/3})/0.45]} \\ &\quad +\ell(\ell+1)\hbar^2/2\mu_M r^2 \\ &\quad +\begin{cases} \frac{Z_P Z_T e^2}{R_C} & \text{for } r > R_C \\ \frac{Z_P Z_T e^2}{R_C}(\frac{3}{2}-\frac{1}{2}\frac{r^2}{R_C^2}) & \text{for } r < R_C \end{cases} \end{aligned}$$

with $R_C = 1.2A_T^{1/3}$.

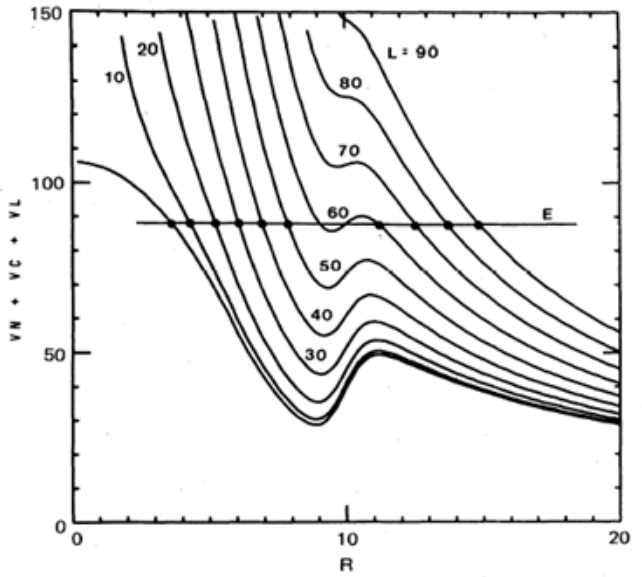

FIG. 1. For the system $^{18}O + ^{120}Sn$ and the potential of Table I the sum of the nuclear, Coulomb, and centrifugal potentials are shown for the values of angular momentum l indicated. The lowest curve, corresponding to $l = 0$, is the nuclear + Coulomb potential. The barrier is seen to be ~ 49 MeV. The horizontal line marks $E_{cm} = 87$ MeV, corresponding to a lab energy of 100 MeV. The turning points for various l are marked by dots. Note the discontinuity occurring at the critical $l_c \sim 57$.

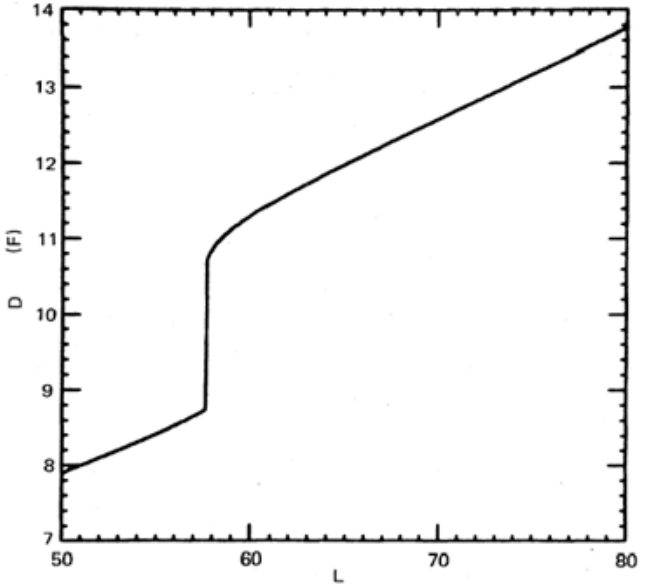

FIG. 2. The variation of the penetration depth or distance of closest approach D as a function of angular momentum for 100 MeV lab energy $^{18}O + ^{120}Sn$. The nuclear potential is that of Table I.

name of "folded interactions" which we should prefix by "frozen configuration." At distances for which appreciable overlap of the two densities occurs, such a folded potential

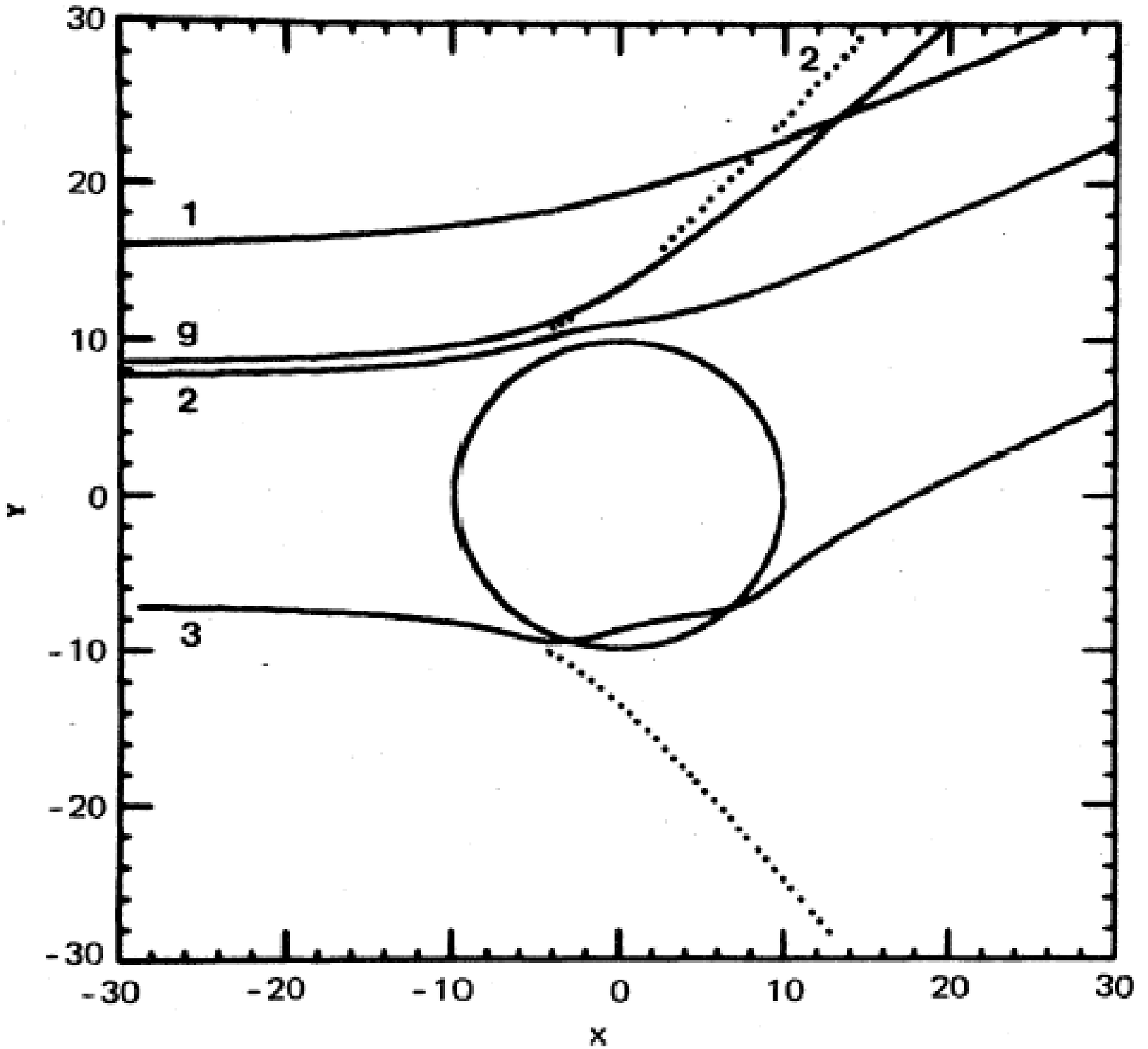

FIG. 3. Four classical orbits in the potential of Table I are plotted, three of which, having impact parameters 1, 2, and -3, $(3 < 2)$ scatter to the same angle θ. The orbit g is the grazing one. The circle marks the half-value of the Woods–Saxon nuclear potential. The orbits are for ^{18}O scattered by ^{120}Sn at 100 MeV lab energy. Dotted lines show pure Coulomb orbits. The scale is in Fermi.

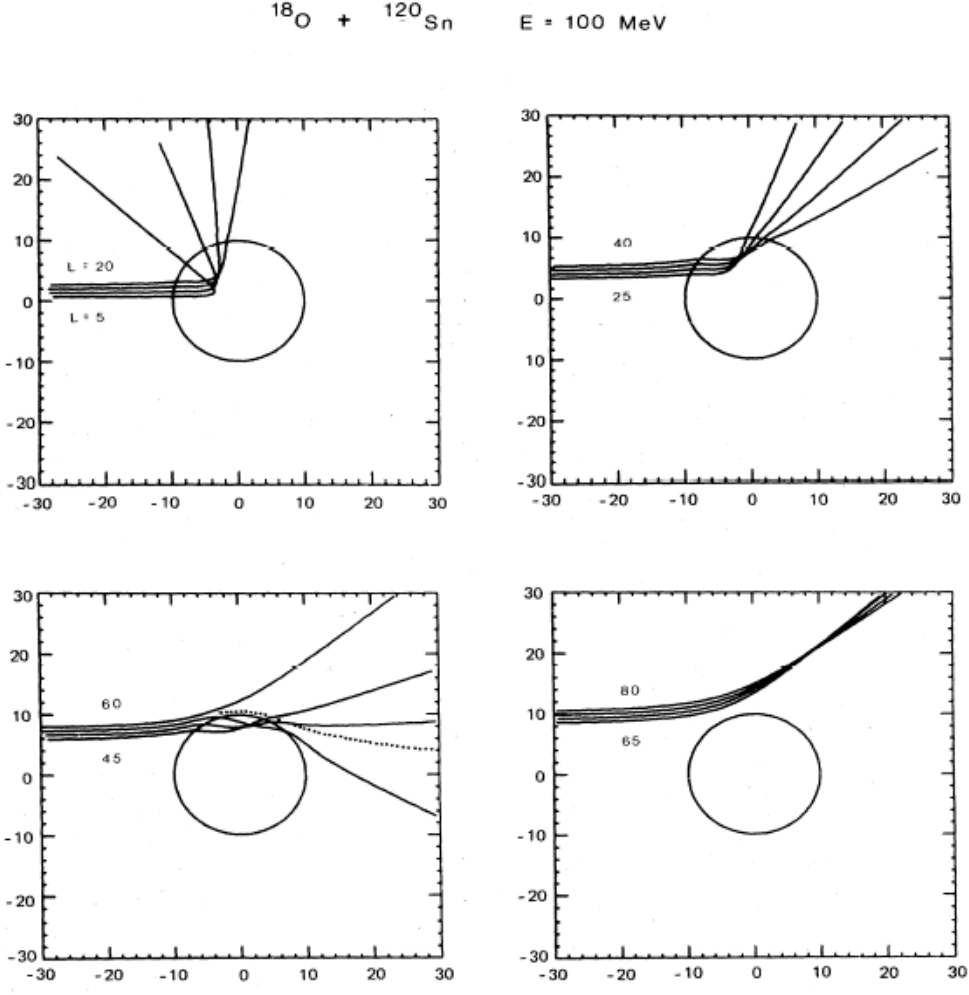

FIG. 5. Some trajectories in the potential of Table I, at intervals of $l = 5$ for 100 MeV ^{18}O scattered from ^{120}Sn. The circle marks the half-value of the nuclear potential. An additional skimming orbit is shown by dotted line.

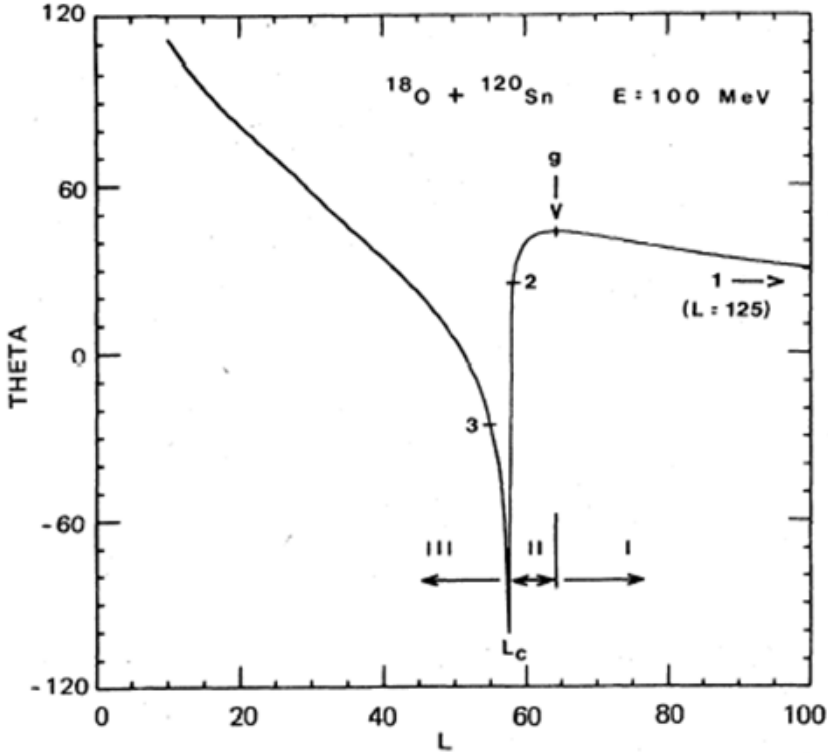

FIG. 6. Deflection function from which the classical scattering angle of a trajectory with angular momentum l can be read for 100 MeV $^{18}O + {}^{120}Sn$. Points on the function corresponding to the four orbits of Fig. 3 are marked. The back scattering for small l is caused by the repulsive Coulomb core, Fig. 1, which at this energy is not surmounted. The singularity occurs at the critical angular momentum l_c. The three regions I, II, and III are discussed in the text. The grazing angle θ_g, which is the maximum to which nonpenetrating orbits can scatter, is about 43°.

2) Find the height of Coulomb barrier, E_b and radial distance of Coulomb barrier, R_b.

3) Extract the radial distance of the turning points for various ℓ, from the figure obtained from the previous problem and draw the radial distance (penetration depth) as a function of angular momentum.

4) Find the angular momentum, ℓ_t, where the turning point changes abruptly, and the corresponding radial distance R_t.

5) Use the imaginary potential in the optical model calculation

$$W(r) = -\frac{15.0}{1+\exp[(r-1.31(A_T^{1/3}+A_P^{1/3})/0.45]}$$

and calculate the amplitude of the S-matrix in terms of ℓ for the elastic scattering. Find the angular momentum and its corresponding radius R_S at which $|S| = 1/2$ occurs.

6) Evaluate the nuclear radius $R_N = 1.31(A_T^{1/3} + A_P^{1/3})$.

7) The grazing distance R_{gr} is known to be

$$R_{gr} = 1.12(A_P^{1/3} + A_T^{1/3}) - 0.94(A_P^{-1/3} + A_T^{-1/3}) + 3.0$$

in fm unit. Evaluate the grazing distance, grazing angle, and grazing angular momentum.

8) Discuss physics of R_b, R_t, R_S, R_N and R_{gr}.

For the answer, consult with the paper by N. K. Glendenning, *Rev. Mod. Phys.*, **47**, 659 (1975).

2 Qualitative characteristics of elastic scattering experiments

2.1 Angular distributions

2.1.1 Projectile dependence

Elastic scattering on ^{58}Ni (Fig. 11.1 upper panel.)

Projectile	E_{lab}	Characteristics	Pattern
Proton	10	Oscillatory	
Proton	40	More oscillatory	
alpha	40	Decreasing Oscillatory	Fraunhofer
^{16}O	160	Monotonous decrease	Fresnel

Reflection coefficients, $\eta_\ell = |S_\ell|$. (Fig. 11.1 lower panel.)

Projectile	E_{lab}	$\lvert S_\ell\rvert = 1$	Low ℓ behavior
Proton	10	6	contributing
Proton	40	10	contributing a lot
alpha	40	20	still contributing
^{16}O	160	100	no reflection (absorption)

Homework #7: 1. Fill out the following table.

Characteristic values

Projectile	E_{lab}	e_{lab}	k	a	η
Proton	10				
Proton	40				
alpha	40				
^{16}O	160				

Two basic influences are present.

1) Short range attractive nuclear potential causes
   refraction and reflection of incident waves
   at the target nucleus surface.
2) Strong absorption resulting from nonelastic collisions.

There are two cases depending on the above two basic influences.

1) Two proton cases;
   a) The diffraction pattern by the attractive nuclear potential at the nuclear surface.
      (The Coulomb force is weak.)
      (The similar one can be seen in the neutron scattering.)
   b) The 40 MeV case has more oscillatory.
      ($|P_\ell(\cos\theta)|^2$ has $(\ell+1)$ maxima from 0 to π, and
      the successive maxima length is π/ℓ on average.)
   c) The grazing angular momentum would just be $\ell_{gr} = kb$. (Weak Coulomb)

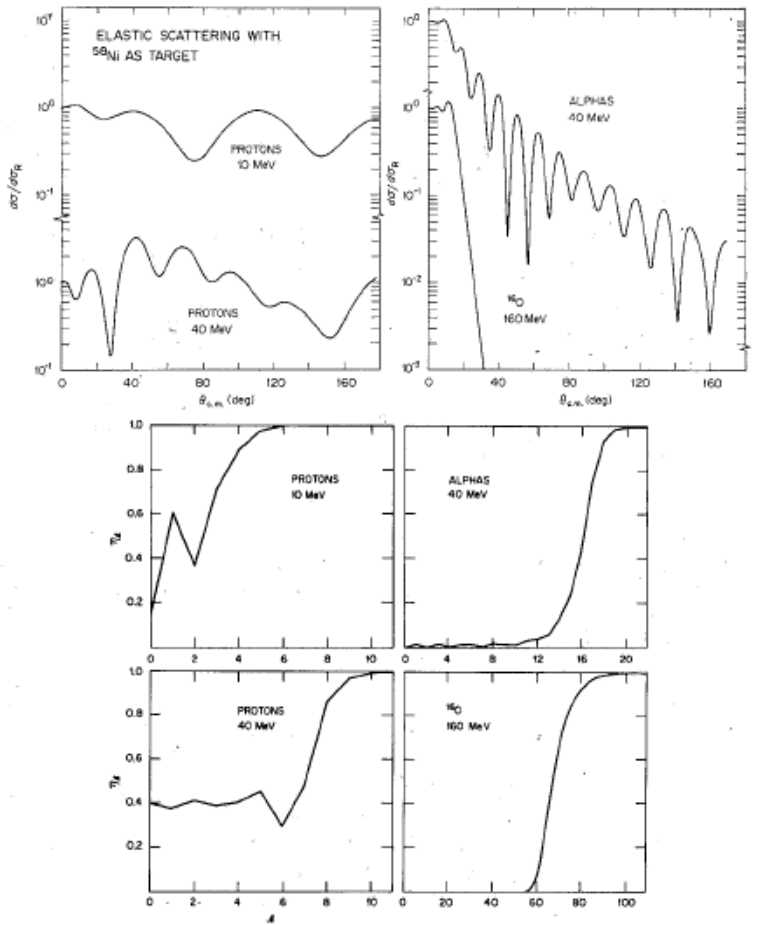

FIG. 11.1. Some typical examples of (a) the differential cross sections (in ratio to the Rutherford cross section), and (b) the reflection coefficients for the elastic scattering of protons, alphas, and ^{16}O ions with energies of 10 MeV per nucleon, and also protons of 40 MeV. Note the changes in scale for the angular momenta.

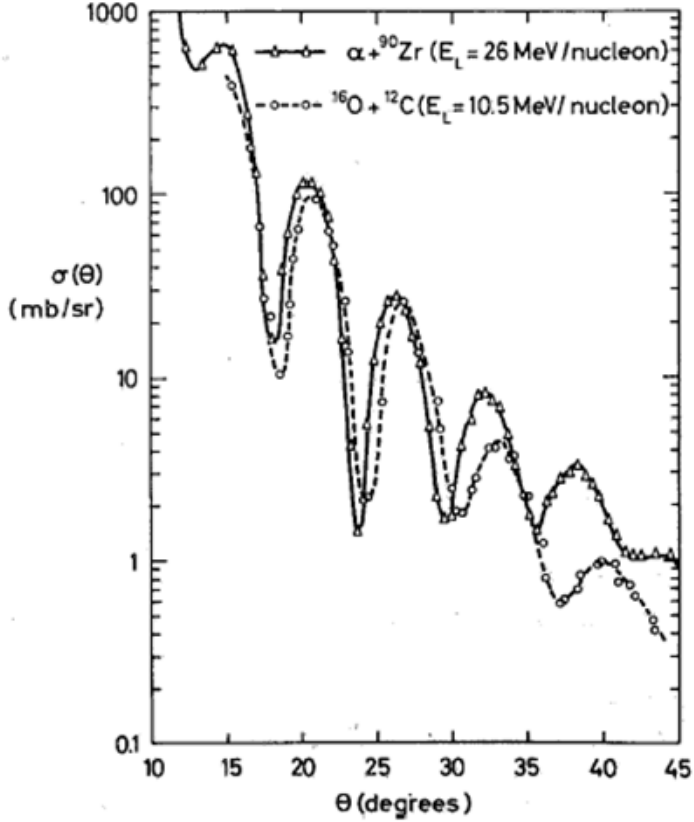

FIG. 11.2. Example of two nearly homomorphic differential cross sections with $n \approx 2.4$ and $\lambda_g \approx 32$. The curves are merely drawn through the experimental points. (From Frahn 1972.)

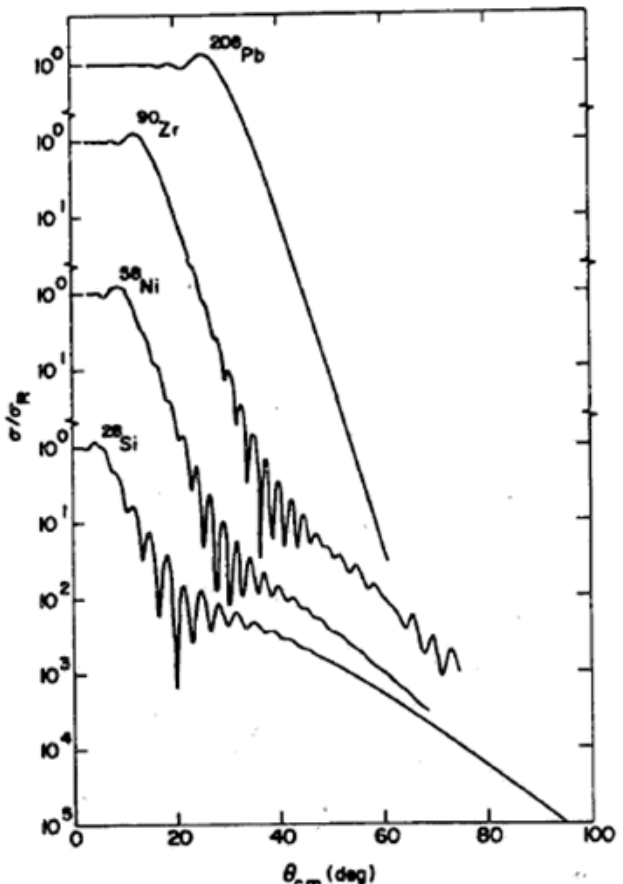

FIG. 11.13. Comparison of cross sections predicted by an optical model for the scattering of 200 MeV ^{16}O from various targets, showing the decrease in importance of Fraunhofer interference as the Coulomb repulsion becomes stronger. (From Goldberg and Smith 1974.)

2) The other two cases (α and ^{16}O);
   a) Strong absorption is dominated after θ_{gr}, and causes rapid decrease in the large scattering angles.
   b) The Coulomb force is strong and the grazing angular momentum should be obtained from the Coulomb scattering formula.
   c) Scattering is primarily diffractive. (Fraunhofer-like and Fresnel-like)

Homework #7: 2. The grazing distance R_{gr} is known to be

$$R_{gr} = 1.12(A_P^{1/3} + A_T^{1/3}) - 0.94(A_P^{-1/3} + A_T^{-1/3}) + 3.0$$

in fm unit. Evaluate the grazing distance, grazing angle, and grazing angular momentum for 4 different systems. Discuss physics.

2.1.2 Fraunhofer-like and Fresnel-like diffraction

1) Fresnel-like diffraction (^{16}O case)
   a) When the impact parameter is large, the scattering is due to the Coulomb force
   b) When b becomes sufficiently small, the two nuclei make contact.
   The short-ranged nuclear interaction begins to act, and removes flux from the elastic channel, and the elastic cross section falls.
   c) Diffraction by the edge of a black sphere.
   (See the next section.)
   It is only for peripheral collisions, where the transition from Rutherford scattering to essentially complete absorption is taking place, that the refractive effects of the real nucleus-nucleus potential can play a role.

2) Quarter-point recipe for Fresnel-like diffraction
   a) A characteristic interaction radius $R_{\frac{1}{4}}$
   It is usual to choose the grazing angle to be the angle $\theta_{\frac{1}{4}}$ at which the cross section has fallen to one quarter of the Rutherford value.
   b) This angle can be associated with an angular momentum $\ell_{\frac{1}{4}}$
   $$\ell_{\frac{1}{4}} = \eta \cot(\tfrac{1}{2}\theta_{\frac{1}{4}})$$
   c) A characteristic interaction radius $R_{\frac{1}{4}}$ which is taken to be the distance of closest approach,
   $$kR_{\frac{1}{4}} = \eta + [\ell_{\frac{1}{4}}^2 + \eta^2]^{1/2} = \eta\{1 + \csc(\tfrac{1}{2}\theta_{\frac{1}{4}})\}.$$

3) Fraunhofer-like diffraction (α case)
   a) As E_{lab} increases relative to the Coulomb barrier, diffraction still dominates the the scattering when there is strong absorption, but its character changes to that of the Fraunhofer type with an oscillatory angular distribution.
   b) The Coulomb field is no longer very effective, the wavelength of projectile gets shorter, interference occurs between waves diffracted around opposite edges of the target. This interference characterizes Fraunhofer-like.

   c) The separation $\Delta\theta$ of successive maxima or minima gives a measure of $\ell_g \sim \pi/\Delta\theta$ which can then be used to define R_g.

4) Distinctions between diffraction patterns.
   a) Prerequisite - large $\ell_g \gg 1$.
   b) $\eta \gg 1$, Fresnel-like scattering
   $\eta \leq 1$, Fraunhofer-like scattering

5) An example of α+^{90}Zr and ^{16}O + ^{12}C systems.
a) $\eta \approx 2.4$ and $\ell_g \approx 32$ for both systems.
b) Fig. 11.2 shows similar angular distributions. (Fraunhofer-like scattering)

2.1.3 Energy and target dependence

Homework #7: 3. Fill out the table for the ^{16}O scattering on the following targets and lab energies.

Target	E_{lab}	e_{lab}	μ_M	k	a	η	R_{gr}	ℓ_{gr}
^{28}Si	40							
^{28}Si	80							
^{28}Si	120							
^{28}Si	200							
^{208}Pb	200							
^{90}Zr	200							
^{58}Ni	200							
^{28}Si	200							

Use the grazing distance R_{gr} given in the Homework #6.3. Discuss the angular distributions of each system in terms of energy dependence and target dependence, and consult with Figs. 11.1, 11.13 and 11.14.

2.2 Reflection coefficients and strong absorption

Further insight is obtained by studying the elastic partial-wave S-matrix elements S_ℓ, which enter expression for the nuclear part of the scattering amplitude

$$\begin{aligned} f(\theta) &= \frac{i}{2k}\sum_\ell (2\ell+1)(1-e^{2i\sigma_\ell}S_\ell)P_\ell(\cos\theta) \\ &= f_C(\theta) + \frac{i}{2k}\sum_\ell (2\ell+1)e^{2i\sigma_\ell}(1-S_\ell)P_\ell(\cos\theta) \end{aligned}$$

where $f_C(\theta)$ is the Coulomb or Rutherford amplitude. We also define

$$S_\ell = \eta_\ell e^{2i\delta_\ell}, \quad 0 \le \eta_\ell \le 1$$

where the reflection coefficients η_ℓ and the nuclear phase shifts δ_ℓ are both real. The η_ℓ for the cross sections illustrated in Fig. 11.1 are shown in the lower panel of that figure.

Strong absorption in a particular partial-wave means that $\eta_\ell \approx 0$ for that wave; essentially, all the flux with angular momentum ℓ is removed from the elastic channel. The idea of strong-absorption scattering is mainly useful when this happens over a fairly large range of ℓ values. The prototype of strong-absorption model is the *sharp-cutoff model* for the S_ℓ:

$$S_\ell = \begin{cases} 1, & \ell > L_c \\ 0, & \ell \le L_c \end{cases}$$

Classically, this corresponds to assuming that all systems that approach more closely than some critical distance $d = R_c$ are completely absorbed, that is, always scattered into some nonelastic channel. This is made explicit if we consider the absorption cross section implied by the S-matrix.

$$\begin{aligned} \sigma_A &= \frac{\pi}{k^2}\sum_{\ell=0}^{L_c}(2\ell+1) \\ &\approx \frac{\pi}{k^2}(L_c+\frac{1}{2})^2 \approx \pi R_c^2(1-\frac{2\eta}{kR_c}) \end{aligned}$$

Without the Coulomb field, $\eta = 0$, this is simply the geometrical area. The diverging-lens effect of the Coulomb repulsion makes the strong absorption region look smaller that πR_c^2. Within this model we can identify L_c and R_c with the grazing L_g and R_g.

Because of the finite range of nuclear forces and the diffuse edges of the nuclei, we expect that a more realistic model would be one in which η_ℓ underwent a rapid but smooth transition from 0 to 1 over a relatively small range Δ of ℓ values centered on L_c and in which some account was taken of the phase δ_ℓ. This is the basis of the smoothed-cutoff or parameterized S-matrix model. It is clear that the η_ℓ for the alpha and ^{16}O examples shown in Fig 11.1 behave in this way, whereas those for the proton examples do not.

The light composite nuclei d, t and ^{3}He, scattering from heavier nuclei, usually exhibit a behavior intermediate between that shown for protons and alphas in Fig. 11.1. Indeed, there are degrees of 'strong absorption', and the alpha example shown in not as strongly absorbed as the heavy-ion example of ^{16}O scattering. By this we refer to the degrees to which the magnitudes of the η_ℓ for the absorbed wave actually approach zero. This is seen more clearly from a logarithmic plot. Fig. 11.5 shows the η_ℓ for a variety of projectiles scattering from ^{27}Al, all with center of mass energies of 10 MeV per nucleon. The abscissa is chosen to be the classical impact parameter $b = (\ell + \frac{1}{2})/k$ instead of ℓ in order to facilitate the comparison. This presentation makes clear that there are differences for small impact parameters; in some sense ^{27}Al is much more 'transparent' to alpha particles than to ^{16}O nuclei.

3 Strong Absorption Models

3.1 Simple diffraction model

The scattering amplitude can be written

$$f(\theta) = \frac{1}{ik}\sum_{\ell}(2\ell+1)P_\ell(\cos\theta)(e^{2i\delta_\ell}-1)$$

Using semi-classical ideas,

a) Replace ℓ by continuous variable L, $\ell + \frac{1}{2} \to L$.
b) Assume continuous variation of phase shift $\delta(L)$.
c) Replace $P_\ell(\cos\theta)$ by an asymptotic form
for large L.
d) Replace $\sum$ by $\int$.

Then

$$f(\theta) \approx \frac{1}{ik}\int LdLJ_0(L\sin\theta)(e^{2i\delta(L)}-1)$$

is valid if $\theta \leq \pi/6$.

1) Fraunhofer scattering

If we set

$$e^{2i\delta(L)} = \begin{cases} 1, & L > L_c \\ 0, & L < L_c \end{cases}$$

(i.e., no scattering if $L > L_c$, and complete absorption if $L < L_c$.), the integral can be evaluated to give the diffractive cross section

$$\sigma_D \approx (kR^2)^2[\frac{J_1(kR\theta)}{kR\theta}]^2$$

where $L = kR$. This diffraction cross section has a characteristic oscillatory behavior with spacing

$$\Delta\theta_D \approx \pi/kR$$

2) Fresnel scattering

We make the large angle approximation in $f(\theta)$:

$$f(\theta) \approx \frac{1}{ik}\int_0^\infty LdL(\frac{2}{\pi L\sin\theta})^{1/2}\cos(\theta-\frac{\pi}{4})(e^{2i\delta(L)}-1)$$

At a scattering angle θ, the main contribution to the integral comes from values of L near L_θ given by

$$2(\frac{d\delta(L)}{dL})_\theta = \pm\theta$$

[Note: This is an equation for L_θ: for Coulomb phase shifts gives $L_\theta = \eta\cot(\theta/2)$.]

Expand $\delta(L)$ about L_θ:

$$\begin{aligned} \delta(L) &= \delta(L_\theta) + (\frac{d\delta}{dL})(L-L_\theta) + \frac{1}{2}(\frac{d^2\delta}{dL^2})(L-L_\theta)^2 + ... \\ 2\delta(L) &= 2\delta(L_\theta) + \theta(L-L_\theta) + \frac{1}{2}(\frac{d\theta}{dL})(L-L_\theta)^2 + ... \end{aligned}$$

Taking out slowly varying functions, and replacing the lower limit of integration by L_c (i.e., sharp cut-off model),

$$f(\theta) \approx \frac{1}{k}\sqrt{\frac{L_\theta}{2\pi \sin\theta}} e^{i\alpha(\theta)} \int_{L_c}^{\infty} dL \exp[\frac{i}{2}(\frac{d\theta}{dL})_\theta (L - L_\theta)^2]$$

This is just the Fresnel integral, shown in Fig. 11.8.

Introducing a new variable x by

$$\begin{aligned} \pi x^2 &\equiv (\frac{d\theta}{dL})_\theta (L - L_\theta)^2 \\ f(\theta) &\approx \frac{1}{k}\sqrt{\frac{L_\theta (dL/d\theta)_\theta}{2\sin\theta}} e^{i\alpha(\theta)} \int_{x_c}^{\infty} dx \exp[\frac{i\pi}{2} x^2] \end{aligned}$$

The integral can be evaluated, replacing $x_c \to -\infty$, i.e., $L_c \ll L_\theta$, as $\sqrt{2}e^{i\pi/4}$. Then

$$\begin{aligned} f(\theta) &\approx \frac{1}{k}\sqrt{\frac{L_\theta (dL/d\theta)_\theta}{\sin\theta}} e^{i\bar{\alpha}(\theta)} \quad \text{where} \quad \bar{\alpha} = \alpha + \frac{\pi}{4}(\frac{d\theta}{dL})_\theta \\ \sigma(\theta) &= |f(\theta)|^2 = \frac{1}{\sin\theta}(\frac{bdb}{d\theta}) \end{aligned}$$

where $L_\theta = kb_\theta$, which is just the classical scattering formula.

Now we note that if x_c is set equal to zero, i.e., $L = L_c$, we have the simple result that at the critical angle θ_c,

$$\frac{\sigma(\theta)}{\sigma_R(\theta)} = \frac{1}{4}$$

which is the origin of the famous "quarter-point" recipe.

4 Optical Model

4.1 Origins of the model

This subsection is a part of the Chapter 17 in "Computers and their role in the physical science", edited by S. Fernbach and A. H. Taub, (Gordon and Breach, 1968). This chapter is written by T. Tamura and W. R. Coker, titled "Computers and the optical model for nuclear scattering".

We would like to explain something of the aim ad nature of the optical model for nuclear scattering and the way in which modern, high-speed computers contribute to the model's application. We first need to summarize some basic facts about atomic nuclei themselves, and a little history of nuclear physics.

The nucleus of an atom is a region about 10^{-12} cm (10 Fermis) in radius, lying at the atom's center. The atom's extra-nuclear region is a "cloud" of electrons confined within a volume roughly 10^{-7}cm in radius. The nucleus of an atom with atomic weight A and Z surrounding electrons contains Z protons and $N = A - Z$ neutrons. Since the protons each have a positive charge equal in magnitude to the negative charge e on an electron, the nucleus has total charge Ze.

The usual notation for a specific nucleus is the chemical symbol for the element (which automatically specifies Z) with a left superscript giving A. For example, ^{90}Zr is the $A = 90$ isotope ($N = 50$) of zirconium ($Z = 40$). The isotope ^{96}Zr has 56 neutrons.

The force acting between two protons, a proton and a neutron, or two neutrons is attractive and to a high degree of accuracy (96%) the same in each case, apart from the additional repulsive electrostatic (or Coulomb) force acting between the like-charged protons. Since protons and neutrons also are similar in mass and other properties, they are usually discussed under the single name, *nucleon*. the nuclear force is found to be almost negligible unless the distance between nucleons is about 10^{-12} cm or less.

Because the nucleons are confined in such a small region by the nuclear force, it is clearly extremely powerful over short distances ($\sim 10^{-13}$ cm). At small enough distances, however, the force between two nucleons must eventually "saturate", and become repulsive, else nuclei would collapse into points. As a result of saturation, the density of nucleons in most nuclei is nearly uniform for the center out to the surface, where it rapidly but smoothly drops to zero. The radius of a nucleus of mass A is proportional to the cube root of A : $R_A = r_0 A^{1/3}$, where r_0 is a constant ($\approx 1.2 \times 10^{-13}$ cm). That is, the nuclear density does not depend on A: since the nuclear volume would be $V_A = (\frac{4}{3})\pi R_A^3 = (\frac{4}{3})\pi r_0^3 A$, the density V_A/A is $(\frac{4}{3})\pi r_0^3$.

Essentially all of our knowledge of the physical properties of nuclei has come from scattering experiments or radioactive decay. In the old days of nuclear physics one had available for observation only the products of the natural radioactive decay of a few heavy ($Z > 82$). Such nuclei decayed, by various routes, into lead (^{208}Pb) by emission of helium (^{4}He) nuclei, - "α rays" or electrons, - "β rays". Very high frequency electromagnetic radiation, "γ radiation", was also observed.

When various types of electrostatic and electromagnetic ion-accelerators became available, it was possible to investigate stable nuclei by bombarding a chemically and isotopically pure sample of material, creating "artificial" radioactivity. A sizable amount of information about the internal structure of nuclei was gained in this way, though the products of the bombardment were still mostly restricted to electrons, and γ rays.

The improvement in particle accelerators following World War II made higher and higher projectile energies available. An electron with a kinetic energy of 100 million electron volts (100 MeV) is, because of the wave nature of matter, localized to within a distance of 10^{-13} cm or less, so that in passing through a thin foil it will be likely to interact with Coulomb field of at most a *single* nucleus. Since the distance within which a particle is localized is inversely proportional to the square root of its kinetic energy, increasing the energy gives us a greater and greater "magnification" and the accelerator becomes a kind of nuclear microscope.

Suppose nucleons themselves are accelerated in such machines at high enough energies (a few

MeV are sufficient, since nucleons have almost 2000 times the mass of electrons) to single out individual nuclei in the target foil. Since the nuclear force is so very powerful, at least over distances comparable to the nuclear radius, it might be expected that usually the nucleon will either be unaffected, passing too far away, or will be sucked into the nucleus, coming too close. In the intermediate case, when the incoming nucleon begins to interact with other nucleons in the near half of the nucleus, those in the back hemisphere are still too far away to influence the projectile's motion. Hence the nuclear collision should be highly complicated, since the many nucleons of the target will tend to interact almost *individually* with the incident nucleon.

Such, at least, was the conjecture made by almost every nuclear physicist prior to a remarkable series of experiments by H.H. Barschall reported in 1952. We cannot go into detail, but the results of Barschall's experiments, in which various nuclei were bombarded with neutrons at energies of an MeV or less, could be explained in a shocking simple way.

Barschall's experimental data could be readily interpreted assuming the existence of a *single* potential with which the incident projectile interacts. A plausible explanation of how the individual strong, short range interaction, of each of the A nucleons in a nucleus can appear as a single interaction, strong over the region of space occupied by the entire nucleus, is far beyond the scope of this discussion. Somewhat inaccurately, we may say that the totality of interactions may be "summed" into an average nucleon-nucleus potential plus a residual nucleon-nucleon interaction, of considerably less strength and range.

An incident nucleon may be deflected from its initial path by this average potential, just as a comet would be deflected by the gravitational potential of the earth, without noticeable complication from the residual interaction. An important point is that all the nucleons contribute to the average potential, and they are *individually* unaffected by interaction of an incoming nucleon with this potential, so that the nucleus itself is quite unaffected, and the deflected nucleon continues on its way without loss of kinetic energy. Such a process is called *elastic scattering*.

A role played by the residual interaction is enormously more complicated and varied. Individual nucleons in the target may, through this interaction, take energy from the incident projectile, one or more target nucleons may be emitted into free space, the projectile may be captured, or other nucleons combined with it as it goes away, and so on. Contributions of this kind from the residual interaction amount to the physical removal, from the beam, of nucleons which would otherwise be elastically scattered or not deflected at all.

Thus a certain number of nucleons neither pass through the target foil undeflected, nor are elastically scattered from it. The situation is quite analogous to the classical problem of optics in which a beam of light is incident upon a translucent object. A certain fraction of the beam is transmitted through the object, another fraction is scattered in various directions, and another fraction is absorbed. The absorption can be included by defining the material's index of refraction to be a *complex* number. The larger the imaginary part of the refractive index is, the more effective is the absorption.

The "optical model" for nucleon-nucleus scattering consists, similarly, in defining a single complex nuclear potential, the real part of which is hopefully the overall average potential we have been discussing, and the imaginary part of which is chosen to give the proper absorption. The residual interaction is otherwise ignored.

In the next section, we give an account of the application of such a model, including only sufficient detail to make clear how and why the use of computers is important. It should be kept in mind throughout all of what follows that the aim of all these labors is to reveal the detailed properties of nuclei.

4.2 Calculation for the model

4.2.1 Basic ideas of nuclear scattering

The Schrödinger equation for the spherically symmetric central field, $V(r)$, can be written as

$$[-\frac{\hbar^2}{2\mu}(\frac{1}{r}\frac{d^2}{dr^2}r) + \frac{\hbar^2\ell(\ell+1)}{2\mu r^2} + V(r)]R_\ell(r) = ER_\ell(r) \tag{1}$$

where μ is the reduced mass of the system in amu, and E is the center-of-mass energy in MeV. We now set

$$R_\ell(r) \equiv \frac{u_\ell(r)}{r} \tag{2}$$

then, $u_\ell(r)$ satisfies

$$\frac{\hbar^2}{2\mu}\frac{d^2u_\ell(r)}{dr^2} + [E - V(r) - \frac{\hbar^2\ell(\ell+1)}{2\mu r^2}]u_\ell(r) = 0 \tag{3}$$

We have learned in the Lecture IV that the scattering amplitude $f(k,\theta)$ is related to the scattering partial phase shifts, δ_ℓ, as

$$f(k,\theta) = \frac{1}{k}\sum_{\ell=0}^{\infty}(2\ell+1)e^{i\delta_\ell}\sin\delta_\ell P_\ell(\cos\theta) \tag{4}$$

where $k = \sqrt{2\mu E}/\hbar$ is the wave number. The differential cross section then becomes

$$\frac{d\sigma}{d\Omega} = |f(k,\theta)|^2 \tag{5}$$

Note that it is in the form of an infinite series, which is in practice not a very handy form unless convergence is very rapid, so that we have to know only the first few δ's. Nonetheless, our problem is now solved in principle once we have found the phase shifts.

If the theoretical differential cross section $|f(k,\theta)|^2$ actually agrees with the experimental cross section, it means that our theoretical calculation has been successful. It is clear that if a potential $V(r)$ is given, a unique set of δ_ℓ can be calculated. Therefore our theoretical task is to find a *good* potential so that a *good* set of phase shifts is obtained, by which is meant that the theoretical differential cross section agrees with experiment. We now need to explain how the phase shifts are calculated, for an arbitrary potential $V(r)$.

Clearly, it is hopeless to look for a simple analytic expansion of $u_\ell(r)$ in terms of known functions, since $V(r)$ must be chosen to describe experimental results, and may have a very complicated functional form. The differential equation for $u_\ell(r)$ cannot be solved analytically unless the function $V(r)$ is of an *extremely* simple form. Thus we must in almost all cases solve equation numerically, with a computer. Our task is then to compute the set of δ_ℓ.

4.2.2 Outline of general procedure for programming

We first rewrite the differential equation as

$$\begin{aligned} u_\ell''(r) &= v(r)u_\ell(r) \\ u_\ell''(r) &= \frac{d^2u_\ell(r)}{dr^2} \\ v(r) &= -\frac{\hbar^2}{2\mu}[E - V(r) - \frac{\hbar^2\ell(\ell+1)}{2\mu r^2}] \end{aligned} \tag{6}$$

Note that the solutions u_ℓ will be complex numbers, since the potential $V(r)$ is to be chosen complex. Let us then assume that we know the solution u_ℓ for two values of r, i.e. at r_0 and r_0+h, where h is assumed very small. We then want to obtain $u_\ell(r)$ at r_0+2h. A possible way to find $u_\ell(r+2h)$ is from the equation

$$u_\ell(r+2h) \approx 2u_\ell(r+h) - u_\ell(r) + h^2 v(r) u_\ell(r+h) \tag{7}$$

That Eq.(7) is a practical and accurate expression can be shown as follows. Let be expand $u_\ell(r_0+h)$ and $u_\ell(r_0+2h)$ in powers of h, using the Taylor expansion. With the abbreviations $u_\ell = u_\ell(r_0), u'_\ell = u'_\ell(r_0) = du_\ell(r_0)/dr, u''_\ell = u''_\ell(r_0) = d^2u_\ell(r_0)/dr^2$, etc., we have

$$u_\ell(r+2h) = u_\ell + 2hu'_\ell + 2h^2u''_\ell + \frac{4}{3}h^3u'''_\ell + \frac{2}{3}h^4u''''_\ell + ...$$

We can now use Eq.(6), which shows that one can rewrite $u''_\ell = vu_\ell (\equiv v(r)u_\ell(r)), u'''_\ell = (vu_\ell)' \equiv d(v(r)u_\ell(r))/dr$, etc. We thus get, for the left hand side of Eq.(7), the expression

$$u_\ell(r+2h) \quad = \quad u_\ell + 2hu'_\ell + 2h^2(vu_\ell) + \frac{4}{3}h^3(vu_\ell)' + \frac{2}{3}h^4(vu_\ell)'' + ... \tag{8}$$

The right hand side of Eq.(7) can also be rewritten in powers of h, and a little algebra shows that it equals

$$u_\ell + 2hu'_\ell + 2h^2(vu_\ell) + \frac{4}{3}h^3(vu_\ell)' + \frac{7}{12}h^4(vu_\ell)'' + ... \tag{9}$$

Comparison of Eq.(8) and Eq.(9) shows that Eq.(7) ceases to be exact only at h^4 and beyond. All such terms will be very small if h was chosen sufficiently small. This means that Eq.(7) can be a very good approximation for $u_\ell(r_0+2h)$, given $u_\ell(r_0+h)$ and $u_\ell(r_0)$.

Now, if we know u_ℓ at two points we can use Eq.(7) to generate the solution at intervals of h for as many points as we need to tabulate $u_\ell(r)$ completely. We always know u_ℓ at one point: $u_\ell(0) = 0$. We can then let $u_\ell(h) = b$, a positive constant. Now we can use Eq.(7) to find $u_\ell(2h)$. The procedure can be mechanically repeated as many times as required, until we have u_ℓ at a value of r very large compared to the distances at which the potential $V(r)$ is large. Thus we have performed an outward integration of the differential equation to just beyond some sufficiently large r, R_m, where $V(R_m) \approx 0$.

We have now numerically generated a large number of values of $u_\ell(r)$, but each is in effect multiplied by an arbitrary constant, through our choice of b. We will have to eliminate this arbitrariness eventually. The values of $u_\ell(r)$ we have generated will be called the internal solution ($r \leq R_m$).

We also want the derivative (or slope) of the internal solution at $r = R_m$. It can be constructed numerically if we have gone two h-steps beyond R_m in the outward integration, by

$$\frac{du_\ell^{(i)}}{dr}]_{r=R_m} \quad \approx \quad \frac{1}{12}[8(u(R_m+h) - u(R_m-h)) - (u(R_m+2h) - u(R_m-2h))] \tag{10}$$

where the (i) superscript will henceforth denote the internal solution. This is the widely-used method of numerical differentiation originated by G. Rutledge.

The differential equations we have considered so far are all of second order; that is, they contain the second derivatives. Such equations are well known to have two linearly independent solutions. We have seen that $F_\ell(kr) = krj_\ell(kr)$, with $j_\ell(kr)$ being the spherical Bessel function, is a solution to radial differential equation with $V = 0$ as discussed in the Lecture III. We thus expect a second solution $G_\ell(kr)$, and indeed $G_\ell(kr) = krn_\ell(kr)$ satisfies the radial equation, with $n_\ell(kr)$ being the spherical Neumann function. It is irregular ($\to \infty$) at the origin, where $j_\ell(kr)$ was regular ($\to 0$), and (to be linearly independent) must approach $\cos(kr - (\ell\pi/2))$ for large r, rather than $\sin(kr - (\ell\pi/2))$.

In the Chapter 2, we can realize that for large r it should be possible to write

$$u_\ell^{(e)}(r) = F_\ell(kr) + C_\ell[G_\ell(kr) + iF_\ell(kr)] \tag{11}$$

for the first term on the right hand side provides the sine, while the second term $\rightarrow \cos(kr) + i\sin(kr) \rightarrow e^{ikr}$. The (e) superscript reminds us that the expansion is useful only external to the potential; i.e. for $r \geq R_m$. The constant C_ℓ must be determined.

Suppose we now match the internal and external solutions by setting equal their magnitude and slope (derivative) at $r = R_m$. Then we will have the function $u_\ell(r)$ at all points, from the origin in steps of h out as far as we feel we must go. Thus

$$\begin{aligned} u_\ell^{(i)}(R_m) = u_\ell^{(e)}(R_m), \qquad & \frac{du_\ell^{(i)}(R_m)}{dr} = \frac{du_\ell^{(i)}(R_m)}{dr} \\ \frac{1}{u_\ell^{(i)}(R_m)}\frac{du_\ell^{(i)}(R_m)}{dr} \quad = \quad & \frac{1}{u_\ell^{(e)}(R_m)}\frac{du_\ell^{(e)}(R_m)}{dr} \equiv \alpha \end{aligned} \tag{12}$$

Now using Eq.(11), the right hand side is known. Further, the division on the left hand side eliminates the arbitrariness of the internal solution by dividing out the arbitrary constant b. Thus only C_ℓ remains unknown. We have

$$\frac{1}{u_\ell^{(i)}}\frac{du_\ell^{(i)}}{dr} = \alpha = \frac{F'_\ell(kr) + C_\ell[G'_\ell(kr) + iF'_\ell(kr)]}{F_\ell(kr) + C_\ell[G_\ell(kr) + iF_\ell(kr)]} \tag{13}$$

which can be easily solved for C_ℓ. We find

$$C_\ell = \frac{-\alpha F_\ell(kr) + F'_\ell(kr)}{\alpha[G_\ell(kr) + iF_\ell(kr)] - [G'_\ell(kr) + iF'_\ell(kr)]} \tag{14}$$

Since we have found C_ℓ, our labor (or that of the computer) is almost at an end, for comparison of Eq.(11) and the solution of radial equation at large distance

$$u_\ell(r \rightarrow \infty) = \sin(kr - \ell\pi/2) + e^{i\delta_\ell}\sin\delta_\ell e^{i(kr-\ell\pi/2)} \tag{15}$$

gives

$$C_\ell = e^{i\delta_\ell}\sin\delta_\ell \tag{16}$$

So we have found what we need. From Eq.(16) may readily be solved for each δ_ℓ.

But how many do we need? Fortunately, we do not need an infinite number. The sum on ℓ in the partial wave expansion can be stopped at some ℓ_{max}, because for $\ell > \ell_{max}, \delta_\ell \approx 0$. The reason for this happy turn of events lies in the effect of the centrifugal barrier term, $\ell(\ell+1)/r^2$ in the radial Schrödinger equation. As ℓ increases, the barrier becomes larger and the incoming particles of angular momentum ℓ cannot come as close to the target. For sufficiently large ℓ, the particle is always so far out that $V \approx 0$ and so $\delta_\ell \approx 0$.

(This situation can also be understood in terms of classical mechanics, if one notices that in order for a particle with a given linear momentum to have a large angular momentum with respect to the force center, it must follow a trajectory which does not pass near the force center.)

4.2.3 Nuclear scattering in the Coulomb field

The computational recipe for optical model calculations is now complete for neutrons. If, however, the projectile is charged, $V(r)$ includes not only the short-range nuclear potential, but the repulsive Coulomb potential between projectile and target nucleus. The Coulomb term, even for large r, is

$$V_C(r) = \frac{Z_1 Z_2 e^2}{r}$$

where Z_1 is the number of protons in the projectile, Z_2 the number in the target, and e the charge on the proton. Note that $rV_C(r)$ does not go to zero as $r \to \infty$. Then in no region of space is an expansion of the form Eq.(11) valid, and the procedure following it is of no use.

However, there is nothing to prevent us from solving the radial Schrödinger equation with $V = V_C$, and indeed the equation can be solved analytically in such a case, although the solutions are by no means as simple as spherical Bessel and Neumann functions. They can be expressed in terms of confluent hypergeometric functions. (See Lecture III-9.)

We can identify the regular and irregular solutions of the Schrödinger equation for the Coulomb field, in much the same way we proceeded above for the case $V(r) = 0$ and $Z_1 = 0$. These functions, which we denote as F_ℓ^C and G_ℓ^C are usually called the Coulomb wave functions, and satisfy

$$\begin{aligned} F_\ell^C(kr) &\longrightarrow_{r\to\infty} \sin(kr - \frac{\ell\pi}{2} + \sigma_\ell) \\ G_\ell^C(kr) &\longrightarrow_{r\to\infty} \cos(kr - \frac{\ell\pi}{2} + \sigma_\ell) \end{aligned} \tag{17}$$

where σ_ℓ is the phase shift due to scattering from the Coulomb potential alone, and is called the Coulomb phase shift, as discussed in Lecture III-10. We assume that as $r \to \infty, kr >> \eta \ln(2kr)$. The Coulomb phase shifts are given by the relation

$$\begin{aligned} \sigma_\ell &= \arg\,\Gamma(\ell + 1 + i\eta) \\ &= \arctan[\frac{\Im\Gamma(\ell+1+i\eta)}{\Re\Gamma(\ell+1+i\eta)}] \end{aligned} \tag{18}$$

where $\eta = (\mu Z_1 Z_2 e^2)/(\hbar^2 k)$, and the function $\Gamma(z)$ is the gamma, or factorial, function. If z is an arbitrary complex number, with real part > 0,

$$\Gamma(z) \equiv \int_0^\infty t^{z-1} e^{-t} dt \tag{19}$$

It is usually most convenient for the computer to construct σ_ℓ for $\ell > 0$ by calculating σ_0 explicitly and obtaining the rest from the recurrence relation

$$\sigma_{\ell+1} = \sigma_\ell + \arctan(\frac{\eta}{\ell+1}) \tag{20}$$

Having the asymptotic forms of $F_\ell^C(kr)$ and $G_\ell^C(kr)$, one can proceed in about the same way as we did for neutrons. The procedure to obtain the internal solution is exactly the same, except that $V(r)$ is replaced by $V(r)+V_C(r)$, so that we wind up with an expression of the same form as Eq.(11), with F_ℓ and G_ℓ replaced, respectively, by F_ℓ^C and G_ℓ^C. Making the same replacements in Eq.(14), we get a new C_ℓ^C which in turn yields a new δ_ℓ^C, through Eq.(15). Summarizing, we obtain

$$\begin{aligned} u_\ell^{(e)}(r) &= F_\ell^C(kr) + C_\ell^C[G_\ell^C(kr) + iF_\ell^C(kr)] \\ u_\ell(r\to\infty) &= \sin(kr - \ell\pi/2 + \sigma_\ell) + C_\ell^C e^{i(kr-\ell\pi/2)+i\sigma_\ell} \\ &= \sin(kr - \ell\pi/2 + \sigma_\ell) + e^{i(\delta_\ell^C+\sigma_\ell)} \sin\delta_\ell^C e^{i(kr-\ell\pi/2)} \end{aligned} \tag{21}$$

Comparison of Eq.(21) with Eq.(15) would seem to indicate that the manipulations connecting Eq.(15) and Eq.(4) can be repeated exactly, merely replacing $e^{i\delta_\ell}\sin\delta_\ell$ by $e^{i(\delta_\ell^C+\sigma_\ell)}\sin\delta_\ell^C$. However, this simple parallelism breaks down, partly because of the additional phase σ_ℓ in $F_\ell^C(kr)$. If we insert $F_\ell^C(kr)$ in place of $u_\ell(kr)$ in the plane wave expansion and sum over ℓ, we cannot obtain a plane wave. Fortunately, part of the remedy is straightforward; we surely have to divide out the extra phase, and so should use $e^{i\sigma_\ell}F_\ell^C$ in the plane wave expansion. Hence we have to multiply each term of Eq.(21) by $e^{i\sigma_\ell}$.

Unfortunately, we still will not have a plane wave as leading term, because $F_\ell^C(kr)$ is itself a complete scattering solution, and must contain both the incident plane wave and an outgoing spherical wave due to the Coulomb-field scattering alone. As a result, substituting $e^{i\sigma_\ell}F_\ell^C(kr)$ into the plane wave expansion gives

$$\sum_{\ell=0}^{\infty}\frac{e^{i\sigma_\ell}F_\ell^C(kr)}{r}Y_\ell^0(\theta) \;=\; e^{i(kz-\eta\ln(r-z))}(1-\frac{\eta^2}{ik(r-z)})+\frac{f_C(\theta)}{r}e^{i(kr-\eta\ln(2kr))} \tag{22}$$

The first term on the right hand side of Eq.(22) indeed resembles a plane wave for large z, although it is distorted by the Coulomb field, through the terms depending on η. However, the second term is the expected Coulomb-scattered outgoing spherical wave, also distorted except at large r (as $r\to\infty, kr >> \eta\ln(2kr)$).

Hence, the analog of Eq.(4) for the full scattering amplitude will now have the form

$$f(k,\theta) \;=\; f_C(k,\theta)+\frac{1}{k}\sum_{\ell=0}^{\infty}\hat{\ell}^2e^{2i\sigma_\ell}e^{i\delta_\ell^C}\sin\delta_\ell^C P_\ell(\theta) \tag{23}$$

with $\hat{\ell}^2=2\ell+1$. The amplitude $f_C(\theta)$ can be expressed in a fairly simple analytic form,

$$f_C(\theta)=\frac{\eta}{2k\sin^2(\theta/2)}\exp[-i\eta\ln(\sin^2(\theta/2))+2i\sigma_0] \tag{24}$$

and is usually called the Rutherford scattering amplitude, after Ernest Lord Rutherford (1871-1937), whose studies of the scattering of low-energy helium nuclei from thin gold foils in fact led to the hypothesis of the nuclear atom.

Evidently, when $V(r)=0, f(k,\theta)=f_C(\theta)$, since $\sin\delta_\ell^C=0$ in Eq.(23). We can identify $f_C(\theta)$ as the scattering amplitude due to the Coulomb field alone, as represented by V_C. If, on the other hand, $V_C=0$ and $V(r)\neq 0$, Eq.(23) is identical to Eq.(4), since $\sigma_\ell=0, f_C(\theta)=0$, and $\delta_\ell^C=\delta_\ell$.

4.2.4 Complex potential, S-matrix, and T-matrix

The added phase shift δ_ℓ^C will be complex if the corresponding potential $V(r)$ is complex. Physically, the imaginary part of $V(r)$ means absorption of flux out of the elastic channel into nonelastic channels. (See Lecture III-3.) Consequently, the amplitude of outgoing elastic wave may be less than unity.

$$\Im\delta_\ell^C\geq 0 \tag{25}$$

The scattering matrix, S_ℓ, is defined as

$$S_\ell \;\equiv\; \exp(2i\delta_\ell^C)=\eta_\ell\exp(2i\delta_\ell) \tag{26}$$

$$\eta_\ell \;=\; |S_\ell|,\quad \delta_\ell=\arg S_\ell \tag{27}$$

which are real. The η_ℓ are sometimes called reflection coefficients. Note that in the absence of the additional potential we have $\delta_\ell=0$ and therefore $S_\ell=\eta_\ell=1$.

The S_ℓ is related C_ℓ as

$$\begin{aligned}
S_\ell &= e^{2i\delta_\ell^C}=\cos 2\delta_\ell+i\sin 2\delta_\ell\\
&= \cos^2\delta_\ell-\sin^2\delta_\ell+i2\sin\delta_\ell\cos\delta_\ell\\
&= 1-2\sin^2\delta_\ell+i2\sin\delta_\ell\cos\delta_\ell\\
&= 1+2i\sin\delta_\ell(i\sin\delta_\ell+\cos\delta_\ell)\\
&= 1+2i\sin\delta_\ell e^{\delta_\ell}\\
&= 1+2iC_\ell
\end{aligned} \tag{28}$$

The scattering amplitude $f(\theta)$ can be written, in terms of S_ℓ, as

$$f(k,\theta) = f_C(k,\theta) + \frac{1}{2ik}\sum_{\ell=0}^{\infty}\hat{\ell}^2 e^{2i\sigma_\ell}(S_\ell - 1)P_\ell(\theta) \tag{29}$$

The T-matrix is defined as

$$T_\ell = 1 - \eta_\ell^2, \quad 0 \leq T_\ell \leq 1 \tag{30}$$

which is often called a transmission coefficient.

4.2.5 Total cross sections for uncharged particles

We can define an integrated elastic cross section for uncharged particles for which $f_C(\theta) = 0$. Using the orthogonality properties of the Legendre polynomials,

$$\sigma_{el} = \int d\Omega(\frac{d\sigma}{d\Omega}) = \frac{\pi}{k^2}\sum_\ell \hat{\ell}^2|1 - S_\ell|^2 \tag{31}$$

The absorption (or also called the reaction) cross section, $\sigma_A(\sigma_R)$ which measures the loss of flux from the elastic channel, is given by

$$\sigma_A = \frac{\pi}{k^2}\sum_\ell \hat{\ell}^2[1 - \eta_\ell^2] = \frac{\pi}{k^2}\sum_\ell \hat{\ell}^2 T_\ell \tag{32}$$

The total cross section, $\sigma_T = \sigma_{el} + \sigma_A$:

$$\sigma_T = \frac{2\pi}{k^2}\sum_\ell \hat{\ell}^2[1 - \Re S_\ell] = \frac{4\pi}{k}\Im f(\theta = 0) \tag{33}$$

according to the well-known optical theorem. There is a theorem equivalent to the above equation for charged particles

$$(\sigma_{el} - \sigma_R) + \sigma_A = \frac{4\pi}{k}\Im f(\theta = 0) \tag{34}$$

$$(\sigma_{el} - \sigma_R) = \int d\Omega[\frac{d\sigma_{el}}{d\Omega} - \frac{d\sigma_R}{d\Omega}] \tag{35}$$

Although both $d\sigma_{el}$ and $d\Omega_R$ are infinite, their difference can be shown to remain finite.

4.3 General properties of optical potentials

4.3.1 A model of the effective interaction

The complicated many-body problem posed by the interaction of two nuclei
→ A simple two-body problem with an effective potential.

We introduce a model wavefunction Ψ_{model}, by truncating the total wave function Ψ to a few basis state,

$$\begin{aligned} \Psi_{model} &= P\Psi \\ \Psi &= P\Psi + Q\Psi \end{aligned}$$

where P and Q are projection operators. The model wave function satisfies a Schrödinger equation

$$(E - \mathcal{H})\Psi_{model} = (E - \mathcal{H})P\Psi = 0$$

with an effective Hamiltonian in the P space,

$$\mathcal{H} = PHP + PHQ\frac{1}{E^{(+)} - QHQ}QHP$$

The effective potential is
a) Complex, if one or more of the eliminated channels is open, with the absorptive imaginary part describing the loss of flux from the model space into these open channels.
b) Nonlocal, because of couplings to the eliminated channels.
c) Energy-dependent, because of couplings to the eliminated channels.
d) Dependent on the particular model space chosen because it has to incorporate all the effects due to the eliminated channels.

The energy-dependency and nonlocality of the optical potential should be such that the dispersion relation which will be discussed Chapter 4 is satisfied but, in practice, this is a weak constraint.

The usefulness of the model;
a) The model contains the basic physics of the scattering process in a quantum-mechanically correct manner.
b) The elastic wave function is not only specified asymptotically, but is continued into the interaction region. Thus direct reaction cross sections can be calculated with DWBA or CC methods.
c) The availability of suitable OM computer codes has been essential for the power and flexibility.

4.3.2 Absorption

a) The only constraint to be placed on a model of $\Im\mathcal{H}$ or $U(r)$ is that it does not cause the emission of more flux than is incident. Since the total angular momentum J is a constant of motion, this demand should be made separately for each J value. Thus the contribution of each J to the reaction (absorption) cross section must be positive, that is

$$\int |\chi^J(r)|^2 W(r) dr \leq 0$$

for each value of J. It is not necessary that $W(r)$ be negative everywhere. Nonetheless, it might be a wise precaution to choose a model $W(r) \leq 0$ for all r to ensure that this condition is always met.

b) The measured scattering for many systems requires the imaginary potential to have a radial shape that is different from the real potential.

c) In some cases, the absorptive potential must be concentrated near the surface. The existence of collective surface modes may enhance surface absorption. For composite systems the possibility of breakup (especially neutron rich nuclei) when the target surface is encountered has the same effect.

4.4 Form of the potentials

4.4.1 Woods-Saxon potential

A functional form for $V(r)$ decreasing smoothly to zero in a surface region of finite thickness is desirable. The functional form which has stood the test of time and is most widely used today, is the form suggested by Woods and Saxon in 1954:

$$\Re[V(r)] = -V_0\{\frac{1}{1+e^{(r-R_0)/a_0}}\}$$

where V_0 is a constant, R_0 is the nuclear radius, and $R_0 = r_0 A_T^{1/3}$ for the light projectile and $R_0 = r_0(A_T^{1/3}+A_P^{1/3})$ for heavy-ions, where $A_T(A_P)$ is the mass number of the target (projectile) and r_0 is called the reduced radius parameter. The length a_0 is the half-width of the surface region, and is usually called the diffuseness.

The imaginary, absorptive, term of $V(r)$ is not very clearly restricted in radial form by experiment; two common forms taken are

$$\begin{aligned}\Im[V(r)] &= -W_0\{\frac{1}{1+e^{(r-R_I)/a_I}}\}, \quad \text{or} \\ &= -W_0\{\frac{4e^{(r-R_I)/a_I}}{(1+e^{(r-R_I)/a_I})^2}\}\end{aligned}$$

where $R_I = r_I A_T^{1/3}$, with $r_I \neq r_0$ in general, but both usually on the order of 1.2 Fermis. Again, W_0 is a constant and a_I is the diffuseness of the surface region.

The angular distribution of the scattered particles is by no means the sole measurable object of an optical model calculation. The framework we have sketched can also give the total cross section, i.e. the angular distribution integrated over all possible outgoing directions for neutrons - for protons, the total cross section is infinite, because of the presence of the Coulomb repulsion even at large distances. More important, the optical model potential can be used to predict the *polarization* of elastically scattered particles, as we discussed in the previous section, and the result can be compared with the numerical tables for $P(\theta)$ resulting from double-scattering experiments.

In order to describe such experiments, a term coupling the spin and orbital angular momentum must be included in the optical potential, as discussed in V-5. The simplest such potential is $(\vec{\ell}\cdot\vec{s})V_{SO}(r)$, usually taken to have the form

$$2(\frac{\hbar}{m_\pi c})^2\frac{V_{SO}}{r}(\vec{s}\cdot\vec{\ell})\frac{d}{dr}[\frac{1}{1+\exp(\frac{r-R_{SO}}{a_{SO}})}]$$

where V_{SO} is a constant, m_π is the mass of pion. This term is usually called the "Thomas term".

Adding the various terms, Eq.(27), (28) and (29), we have the complete nuclear optical potential. While the elastic scattering cross section is particularly sensitive to terms Eq.(27) and (28), the polarization is solely produced by Eq.(29). Hence both types of experiments are required in general to test a given potential.

The widely used optical potential part has been assumed to be of Woods-Saxon type,

$$\begin{aligned}U(r) &= -V_0 f_0(r) - \bar{\lambda}_\pi^2(\vec{\sigma}\cdot\vec{\ell})V_{SO}f_{SO}(r) + V_{Coul} \\ &\quad -i[W_I f_I(r) + 4W_S f_S(r)]\end{aligned}$$

where $\bar{\lambda}_\pi = \hbar/m_\pi c = \sqrt{2}$, and

$$f_0(r) = \frac{1}{1+\exp[(r-R_0)/a_0]}$$

$$
\begin{aligned}
f_I(r) &= \frac{1}{1+\exp[(r-R_I)/a_I]} \\
f_S(r) &= \frac{1+\exp[(r-R_S)/a_S]}{\{1+\exp[(r-R_S)/a_S]\}^2} \\
f_{SO}(r) &= \frac{1}{a_{SO}r}\frac{1+\exp[(r-R_{SO})/a_{SO}]}{\{1+\exp[(r-R_{SO})/a_{SO}]\}^2}
\end{aligned}
$$

where $R_i = r_i(A_1^{1/3} + A_T^{1/3})$ with $i = 0, I, S, SO$ and r_i is called the reduced radius parameter.

The Coulomb potential V_{Coul} is usually approximated by the potential between a point charge $Z_P e$ and a homogeneously charged sphere with charge $Z_T e$ and radius $R_C = r_C(A_1^{1/3} + A_T^{1/3})$:

$$
V_{Coul}(r) = \begin{cases} \frac{Z_P Z_T e^2}{R_C} & \text{for } r > R_C \\ \frac{Z_P Z_T e^2}{R_C}(\frac{3}{2} - \frac{1}{2}\frac{r^2}{R_C^2}) & \text{for } r < R_C \end{cases}
$$

4.4.2 (Homework Set #8) Heavy-ion scattering in the Woods-Saxon potential

G. R. Satchler *Phys. Lett.*, **55B**, 167 (1975) obtained an excellent fit with the optical model for the elastic scattering on ^{12}C + ^{208}Pb at 96 MeV. Reproduce his results with the optical model program "VENUS0".

4.4.3 Folding potential

The philosophy behind the double-folding model is based on the fact that the scattering is dominated by the real potential at large distances. In this low-density overlap region one can assume that nucleons interact as if they were free. Then

$$
V(\vec{r}) = \int d\vec{r}_1 \int d\vec{r}_2 \rho_T(\vec{r}_1)\rho_P(\vec{r}_2)v(\vec{r}_{12})
$$

where ρ is the matter distribution, and $v(r_{12})$ is the nucleon-nucleon interaction with $\vec{r}_{12} = \vec{r} + \vec{r}_2 - \vec{r}_1$. Because there is integration over two densities, this is called the double-folding model. If the projectile is a single nucleon, i.e., $\rho_P = \delta(\vec{r}_2)$, this expression reduces to the single-folded form

$$
V(\vec{r}) = \int d\vec{r}_1 \rho_T(\vec{r}_1)v(|\vec{r} - \vec{r}_1|)
$$

This folding integrals can be evaluated through usual multipole expansions.

The folding integrals in the momentum space makes easier than directly doing the folding integrals in the coordinate space, since the Fourier transform of the folded quantity is the simply the product of the transforms of the individual component functions.

We define the Fourier transform of a function $f(\vec{r})$ by

$$
\begin{aligned}
\bar{f}(\vec{k}) &= \int d\vec{r} \exp(i\vec{k}\cdot\vec{r}) f(\vec{r}) \\
f(\vec{r}) &= (2\pi)^{-3} \int d\vec{k} \exp(-i\vec{k}\cdot\vec{r}) \bar{f}(\vec{k}) \\
\delta(\vec{k}) &= (2\pi)^{-3} \int d\vec{r} \exp(i\vec{k}\cdot\vec{r})
\end{aligned}
$$

The double folding integral becomes

$$
\begin{aligned}
V(\vec{r}) &= \int d\vec{r}_1 \int d\vec{r}_2 \rho_T(\vec{r}_1)\rho_P(\vec{r}_2)v(\vec{r}_{12}) \\
&= (2\pi)^{-3} \int d\vec{k} \exp(-i\vec{k}\cdot\vec{r}) \bar{V}_F(\vec{k}) \\
\bar{V}_F(\vec{k}) &= \bar{\rho}_T(\vec{k})\bar{\rho}_P(-\vec{k})\bar{v}(\vec{k})
\end{aligned}
$$

Likewise the single folding integral becomes

$$\begin{aligned} V(\vec{r}) &= \int d\vec{r}_1 \rho_T(\vec{r}_1) v(|\vec{r} - \vec{r}_1|) \\ &= (2\pi)^{-3} \int d\vec{k} \exp(-i\vec{k} \cdot \vec{r}) \bar{V}_F(\vec{k}) \\ \bar{V}_F(\vec{k}) &= \bar{\rho}_T(\vec{k}) \bar{v}(\vec{k}) \end{aligned}$$

The potentials generated by this model are very deep in the center, typically several hundreds MeV, compared to several tens MeV for the Woods-Saxon potentials.

4.4.4 (Homework Set #9) Heavy-ion scattering in the folding potential

G. R. Satchler *Phys. Lett.*, **55B**, 167 (1975) obtained an excellent fit with the optical model for the elastic scattering on ^{12}C + ^{208}Pb at 96 MeV. Reproduce his results with the optical model program "VENUS0".

4.5 Continuous ambiguities

4.5.1 VR^2 ambiguity for nucleon scattering

Usually, small variations in one part of the potential can be compensated for by small variations in another part so that the scattering is almost unchanged. Then ranges of parameter values may be found to give equally acceptable fits to data. The first of these ambiguities to be recognized was the VR^n ambiguity for nucleon scattering when using a Woods-Saxon type of potential. Small variations in V and R that preserve VR^n = constant (with $n \approx 2$) give similar scattering and hence may give equally good fits to data. It was also noticed that the observed scattering for heavier ions did not distinguish between volume and surface absorption. Interplay between the effects of other optical model parameters was also observed, thus rendering their individual values uncertain. However, many of these ambiguities tended to vanish or at least assume importance as the quality and completeness of the data improved. Doing experiments at higher energies often had the same effect.

4.5.2 Igo ambiguity for heavy-ion scattering

Another continuous ambiguity noted by Igo (1959) for alpha scattering at 40 MeV may arise under conditions of strong absorption. Then, frequently, the scattering (particularly at the lower energies) is sensitive only the tail of the potential so that any set of parameters that leaves this region unchanged will provide agreement with experiment. The Woods-Saxon potentials reduce to simple exponentials at large radii where $(r - R) \gg a$. Then

$$V(r) \rightarrow -(V_0 e^{R_V/a_V}) e^{-r/a_V} - W e^{R_W/a_W} e^{-r/a_W}$$

For given values of a_V and a_W, any combination of V_0 and R_V or W and R_W which yields the same values for parameters will leave $V(r)$ unaltered in this region. Fig. 12.12 shows an example in which varying V and W by two orders of magnitude can be compensated for by varying the radius R in accord with the above equation without significantly changing χ^2. In such cases each part of the potential may be characterized in terms of its value and slope in the vicinity of the strong-absorption radius. This requires at most four parameters, three if the real and imaginary slopes can be taken equal [$a_W = a_V$].

Sometimes the process of fitting data for the scattering of heavier ions seems to be relatively insensitive even to the slope of the potential so that the above equation a range of values of the diffuseness parameters a_V, a_W may be allowed. What is often found is that for a given functional form these equivalent potentials tend cross (i.e., become equal in value) at one radius which is close to the strong absorption radius. Fig. 12.13 provides an example for ^{16}O scattering.

4.6 Nuclear scattering with a spin-orbit force

Now the description of nucleon elastic scattering from a central potential is almost complete. Only one further complication needs to be discussed. Physically, ℓ is quantized *orbital* angular momentum of the incident nucleon, $\ell\hbar$ being comparable to the classical quantity $L = r\mu v \sin\phi$, where ϕ is the angle between $\vec{r}$ and $\vec{v}$. But nucleons also possess an *intrinsic* angular momentum, $\vec{s}\hbar$, of magnitude $\hbar/2$. The intrinsic angular momentum, usually called the spin, can align itself either parallel or antiparallel to a chosen axis. These are the only two possible orientations allowed quantum mechanically.

Inclusion of the spin in the elastic scattering formalism would be trivial were it not for the fact that experiments which allow determination of the "population" of each spin state in a scattered beam revel that the true nuclear potential is able to change the number of nucleons having a given spin orientation. However, the total angular momentum $\vec{j} = \vec{\ell} + \vec{s}$, carried by each partial wave, remains the same, so that if we specify both j and ℓ, we should still be able to expand $f(k,\theta)$ in a form analogous to Eq.(4) or Eq.(24).

Let us be more explicit about the spin effects. Previously, the z-axis has been chosen to be the incident beam direction. We will choose the x-axis as the one along which the spin is to be aligned. In the particular case in which as many particles in the beam have spins along the positive x-axis ("up") as have spins along the negative x-axis ("down"), the beam is said to be *unpolarized*.

As long as the beam is in fact unpolarized, there is nothing special in our choice of the x-axis, and any arbitrary in the $x-y$ plane would work as well, so that the independence of the scattering phenomenon from any choice of azimuthal angle ϕ is retained. But the converse holds also, for we now expect that when the incident beam is *polarized*, so that, for example, more spins point up than down the x-axis, the azimuthal symmetry of the scattering process is lost. The differential scattering cross section measured in the positive y direction ($\phi = (\pi/2)$, "right") will not be the same as that in the negative y direction ($\phi = -(\pi/2)$, "left") even for the same θ and k. This effect is known as the right-left asymmetry of the scattering.

To return to our problems with ℓ, notice that to each value of ℓ, there correspond two values of j, the magnitude of the total angular momentum; namely, $j = \ell + 1/2$ (spin parallel to the direction of $\vec{\ell}$), and $j = \ell - 1/2$ (spin antiparallel). Because the nuclear potential is not quite the same for the two cases, we expect that the nuclear phase shift is not the same. Our expression for $f(k,\theta)$ (Eq.(4) or (24)) is modified considerably, but we will not restate it save to remark that it will have to exhibit two phase shifts for each ℓ, $\delta_{\ell,j=(\ell+1/2)} \equiv \delta_\ell^{(+)}$, and $\delta_{\ell,j=(\ell-1/2)} \equiv \delta_\ell^{(-)}$, which will not in general be equal.

In order that our phenomenological potential $V(r)$ can produce two such sets of phase shifts, it will have to contain a term explicitly coupling $\vec{\ell}$ and $\vec{s}$, having a form such as $(\vec{s}\cdot\vec{\ell})V_{SO}$. We do not have space - and the reader is not likely to have patience - for details, but it will be noted that since $\vec{j} = \vec{\ell} + \vec{s}$, then $\vec{j}^2 = \vec{\ell}^2 + \vec{s}^2 + 2\vec{\ell}\cdot\vec{s}$, so that

$$\vec{\ell}\cdot\vec{s} = (\vec{j}^2 - \vec{\ell}^2 - \vec{s}^2)/2$$

The quantum mechanical magnitudes of $\vec{j}^2, \vec{\ell}^2$ and $\vec{s}^2$ are just $j(j+1), \ell(\ell+1)$, and $s(s+1)$ respectively. Since $s = 1/2$ always, $\vec{s}^2$ is just $3/4$. The reader can satisfy himself that for $j = \ell + 1/2$, $\vec{\ell}\cdot\vec{s}$ becomes ℓ, while for $j = \ell - 1/2$, it is $-(\ell+1)$. The result is that we obtain two equations of the form of Eq.(3), one for each j, with potentials V differing by the magnitude of the constant V_{SO}, since $[(\vec{\ell}\cdot\vec{s})V_{SO}]_{j=\ell+1/2} - [(\vec{\ell}\cdot\vec{s})V_{SO}]_{j=\ell-1/2} = \ell V_{SO} - (\ell+1)V_{SO} = -V_{SO}$. Each of the two equations can be solved in exactly the same way as we discussed previously, and their solutions give, respectively, the two phase shifts $\delta_\ell^{(+)}, \delta_\ell^{(-)}$. When $V_{SO} = 0$, we recover Eq.(4) since the two δ's both become just δ_ℓ.

In the usual scattering experiment, the incident beam is unpolarized, but to be realistic we have to set $V_{SO} \neq 0$. However, the scattering cross section is still independent of ϕ, as we have

explained. The scattered beam will be polarized, to some degree, because of V_{SO}, and we need to say a little about how the polarization is measured.

Assume that we have a *second* target, from which we rescatter the scattered beam. Since the scattered beam is polarized, we expect a left-right asymmetry (ϕ dependence). If the second scatterer does not introduce an unknown quantity, we can calculate the expected asymmetry from the phase shifts $\delta_\ell^{(\pm)}$. The polarization of the nucleons scattered through a certain angle θ relative to the z-axis is

$$P(\theta) = (N_+ - N_-)/(N_+ + N_-)$$

where N_+ is the number of nucleons with spin along the positive x-axis, and N_- is the number with spin along the negative x-axis. The quantity $P(\theta)$ is obtained by rescattering the nucleons from a second target, usually ^{12}C, and measuring the asymmetry. If I_L and I_R are the number of nucleons scattered through a given angle θ' to the left and to the right of the scattered beam axis, then it can be shown that

$$P = [(I_R - I_L)/(I_R + I_L)]P_C^{-1}$$

where P_C is the polarization produced by the second scatterer, and must be known from previous experiments.

4.6.1 (Homework Set #10) Neutron scattering

C. D. Zafiratos, T. A. Oliphant, J. S. Levin, and L. Cranberg, (*Phys. Rev. Lett.*, **14**, 913 (1965)) measured the elastic neutron scattering from ^{209}Bi target at 7 MeV. They also had an excellent fit with the optical model. (See Roy and Nigam's book, p. 379.) Reproduce their results with the optical model program "VENUS".

4.7 Automatic parameter search

We have noticed that a sizable number of parameters in the potential: $V_0, a_0, r_0, W_0, a_I, r_I, V_{SO}, a_{SO}, r_{SO}$, and r_C. Hence the physical labor required in repeating the calculation while varying various parameters until a fit to data is achieved can become immense.

As a result, almost all existing optical model programs contained automatic parameter search routines, which vary a given set of parameters in a specific way to minimize the quantity

$$\chi^2 = \frac{1}{N}\sum_{i=1}^{N}[(\sigma(\theta_i) - \sigma^D(\theta_i))/E^D(\theta_i)]$$

where $\sigma^D(\theta_i)$ is the experimental cross section (or data point) at angle θ_i, $E^D(\theta_i)$ is the experimental error with the data point, $\sigma(\theta_i)$ is the calculated value of the cross section at the same angle, and N is the total number of data points. A considerable budget of ingenuity has been expended on the construction of such search ing subroutines, but they lie far beyond the scope of this lecture.

4.7.1 (Homework Set #11) Parameter search for heavy-ion scattering

J.B. Ball, C. B. Fulmer, E. E. Gross, M. L. Halbert, D. C. Hensley, C. A. Ludemann, M. J. Saltmarsh, and G. R. Satchler (*Nucl. Phys.* , **A252**, 208 (1975)) measured the elastic scattering on ^{16}O + ^{208}Pb at 129.5 MeV. Find a fit with the optical model by using the optical model automatic search program "OPTXSQ".

A Optical model program - VENUS (VENUS0)

A.1 Purpose

The Program VENUS (VENUS0) calculates first the distorted waves, Coulomb phase shifts, and S-matrices for each partial waves and then nuclear elastic scattering cross sections, based on the optical model with (without) the spin-orbit interaction. The optical potential is used of the Woods-Saxon type.

A.2 Subroutines

Name	Function
VENUS(0)	Main program, read input data
OPTMDL(0)	Prepares the optical model calculations
COUPHS	Coulomb phase shifts
POTEN	Various Woods-Saxon potentials
DISWV(0)	Distorted waves and S-matrices for ℓ
COUFT	Coulomb function
ELCROS(0)	Elastic cross sections,
LENGR	Lengdre polynomials
ELETC(0)	Fusion and reaction cross sections

A.3 Input Data

Card # (Format)	Variable Name	Function
1	KTRL(2)	=0; Volume imag. potential for fusion
(24I3)		=1; Volume +surface 1
		=2; Volume +surface 1 + 2
	KTRL(3)	=1: Elastic cross sections
	KTRL(4)	=1; Fusion cross sections
2	KOUT(1)	$\neq$ 0; Output of kinematical values
(24I3)	KOUT(2)	=N; Output of potential values. N equals step
3	TMST	Target mass
(10F7.4)	PMST	Projectile mass
	TZ	Target charge
	PZ	Projectile charge
4	ELABI	Lab system energy
(10F7.4)	XMES	Mesh size
	THMIN	Minimum angle
	THMAX	Maximum angle
	THINC	Angle interval
5	LMAX	Number of Maximum ℓ
(14I5)	NXMAX	Maximum integration range
6,7	VO, AO, RO	OM real parameters
(10F7.4)	WO, AI, RI	Imaginary volume part
	WS1,AIS1,RIS1	Surface imaginary part 1
	WS2,AIS2,RIS2	Surface imaginary part 2
	RC	Coulomb radius parameter
	VSP,ASP,RSP	Spin-orbit parameter

B Automatic parameter search program - OPTXSQ

B.1 Subroutines

Name	Function
OPTXSQ	Main program, read input data
AUTO	Prepares automatic parameter search
CALCUL	Search parameters
CCCTRL	Prepares the optical model calculations
OPT	Calculates the elastic scattering cross sections
POTEN	Various Woods-Saxon potentials
CHISQ	Calculates chi-sqarures
LENGR	Lengdre polynomials
FLGLCH	Calculates Coulomb waves

B.2 Input Data

Card # (Format)	Variable Name	Function	
1	KTRLD(1)	=1; ECM is used.	
(24I3)	KTRLD(5)	=1; Diff. elastic cross section.	
	KTRLD(10)	=1; Chi-square fitting is done.	
	KTRLD(13)	=0; Diff/Ruth are used.	
		=1; Diff. cross sections.	
2	KRLOUT(N)	Output	
3	TMST	Target mass	
(10F7.4)	PMST	Projectile mass	
	TZ	Target charge	
	PZ	Projectile charge	
4	ELABI	Lab system energy	
(10F7.4)	RCUT	Dummy	
	XMES	Mesh size	
	THMIN	Minimum angle	
	THMAX	Maximum angle	
	THINC	Angle interval	
5	LMAX	Number of Maximum ℓ	
(14I5)	MMAX	Number of Maximum m	
	NXMAX	Maximum integration range	
	NANGLR	Number of input angles	
6,7	VO, AO, RO	OM real parameters	
(10F7.4)	WO, AI, RI	Imaginary volume part	
	WS1,AIS1,RIS1	Surface imaginary part 1	
	WS2,AIS2,RIS2	Surface imaginary part 2	
	RC	Coulomb radius parameter	
	VSP,ASP,RSP	Spin-orbit parameter,	*(continued)*

Card # (Format)	Variable Name	Function
8 (24I3)	KTL(N)	Controls auto routine potential for fusion
9 (14I5)	NOVAR	Number of search variables
	IPA(I)	Assigned number of each para. See the next Table
10 (10F9.5)	FKM	Maximum number of iterations
	AKOFF	Desired accuracy
	FCTR	?
	FLAMDA	?
11 (18F4.1)	DY(I)	Weighting factor of each para.
12 (10F8.4)	THETAD(N)	Experimental angles
	SGMEXP(N)	Experimental cross sections
	DSGMEX(N)	Experimental errors

Assigned number of each potential parameter:

Assigned #	Variable Name	Parameter
1	PARAM(1)	VO
2	PARAM(2)	WO
3	PARAM(3)	WS1
4	PARAM(4)	WS2
5	PARAM(5)	RO
6	PARAM(6)	RI
7	PARAM(7)	RIS1
8	PARAM(8)	RIS2
9	PARAM(9)	RCUT
10	PARAM(10)	AO
11	PARAM(11)	AI
12	PARAM(12)	AIS1
13	PARAM(13)	AIS2
14	PARAM(14)	RC
15	PARAM(15)	VS1
16	PARAM(16)	VV1
17	PARAM(17)	VV2

C Double folding potential program -DFPOT

A program for generating the double folding potential is published by J.Cook in the Computer Physics Communication **25** 125-139 (1982).

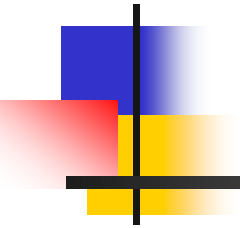

Chap. 3 Elastic Scattering – figures

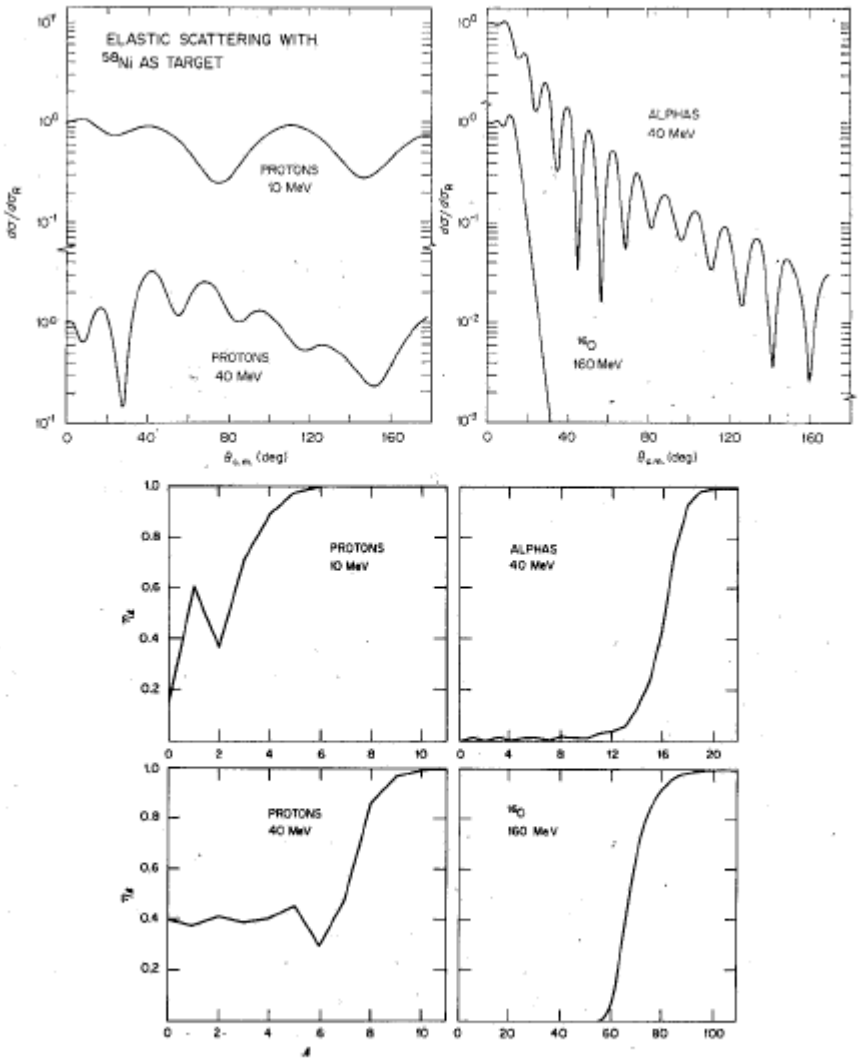

FIG. 11.1. Some typical examples of (a) the differential cross sections (in ratio to the Rutherford cross section), and (b) the reflection coefficients for the elastic scattering of protons, alphas, and ^{16}O ions with energies of 10 MeV per nucleon, and also protons of 40 MeV. Note the changes in scale for the angular momenta.

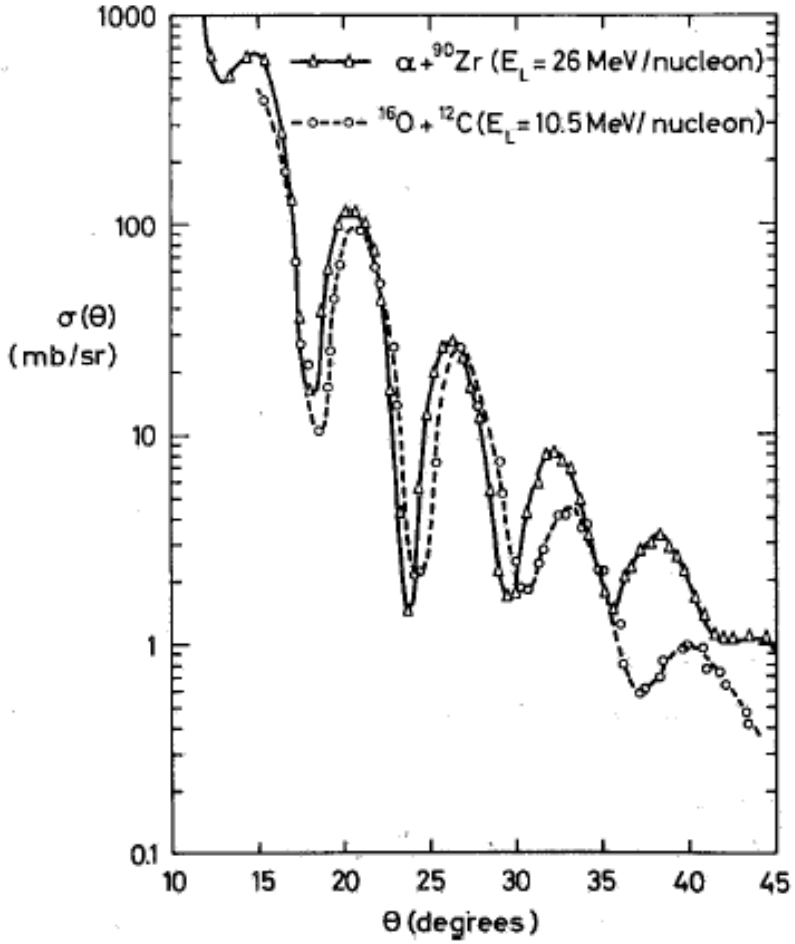

FIG. 11.2. Example of two nearly homomorphic differential cross sections with $n \approx 2.4$ and $\lambda_g \approx 32$. The curves are merely drawn through the experimental points. (From Frahn 1972.)

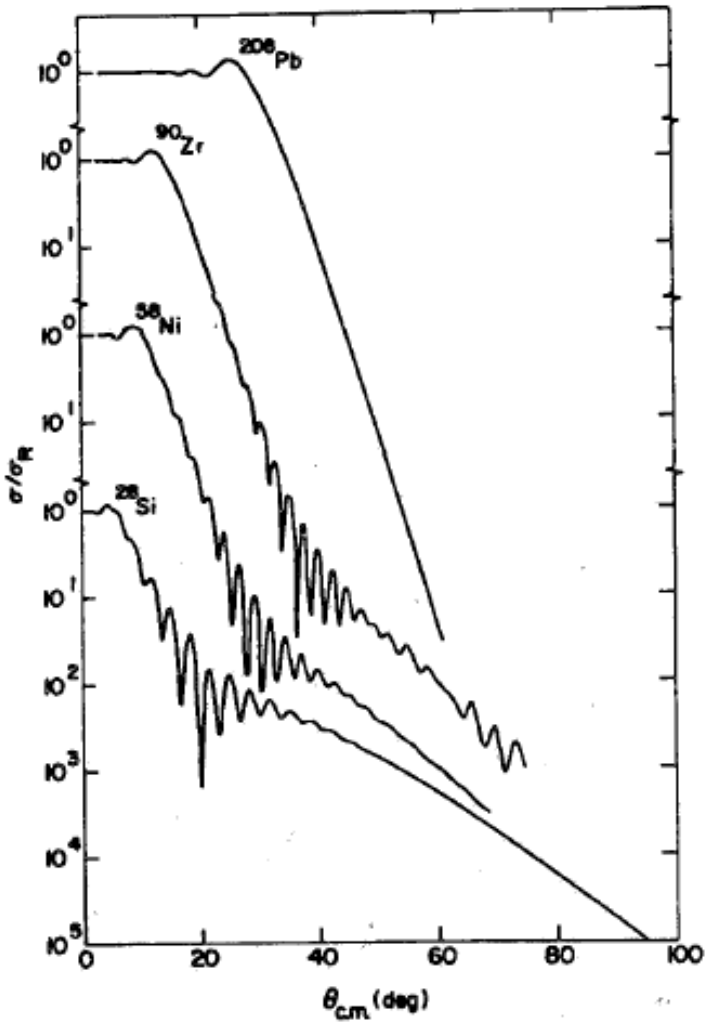

FIG. 11.13. Comparison of cross sections predicted by an optical model for the scattering of 200 MeV ^{16}O from various targets, showing the decrease in importance of Fraunhofer interference as the Coulomb repulsion becomes stronger. (From Goldberg and Smith 1974.)

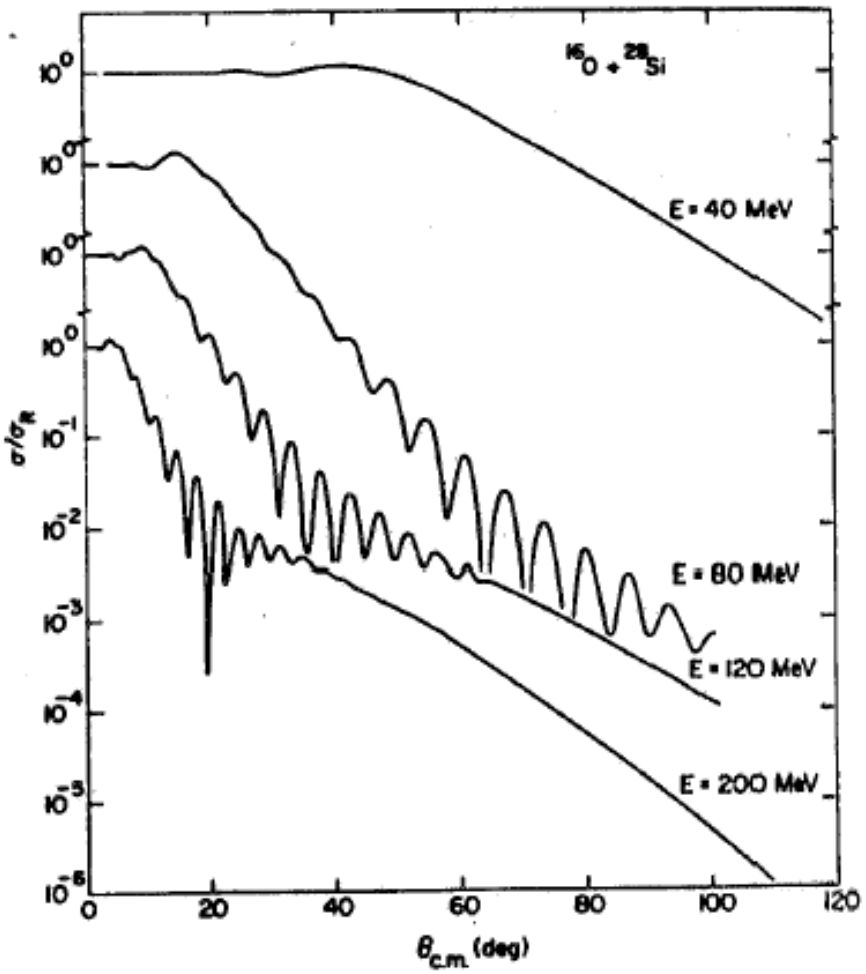

FIG. 11.14. Showing how the importance of Fraunhofer interference increases as the bombarding energy is raised. (From Goldberg and Smith 1974.)

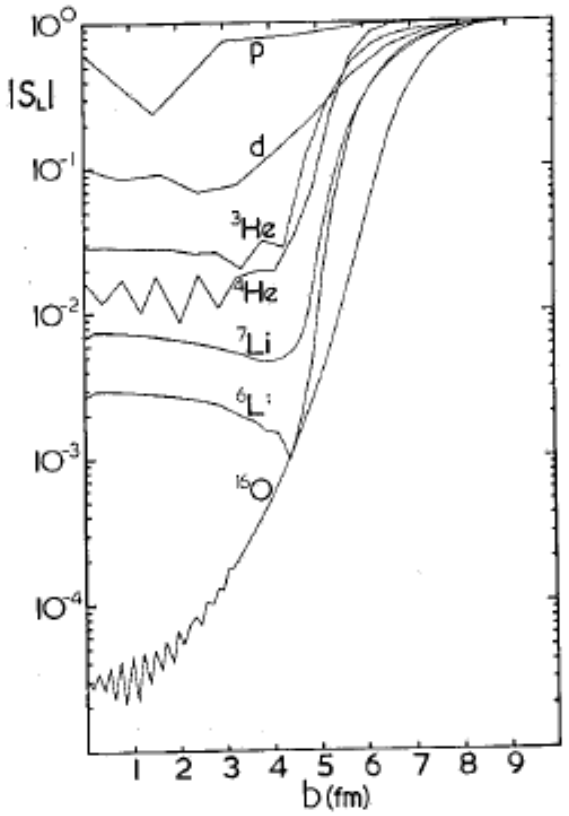

FIG. 11.5. Reflection coefficients obtained from optical-model potentials for various projectiles with energies of 10 MeV per nucleon scattering from ^{27}Al. The abscissa is the semiclassical impact parameter. (From Cook et al. 1980.)

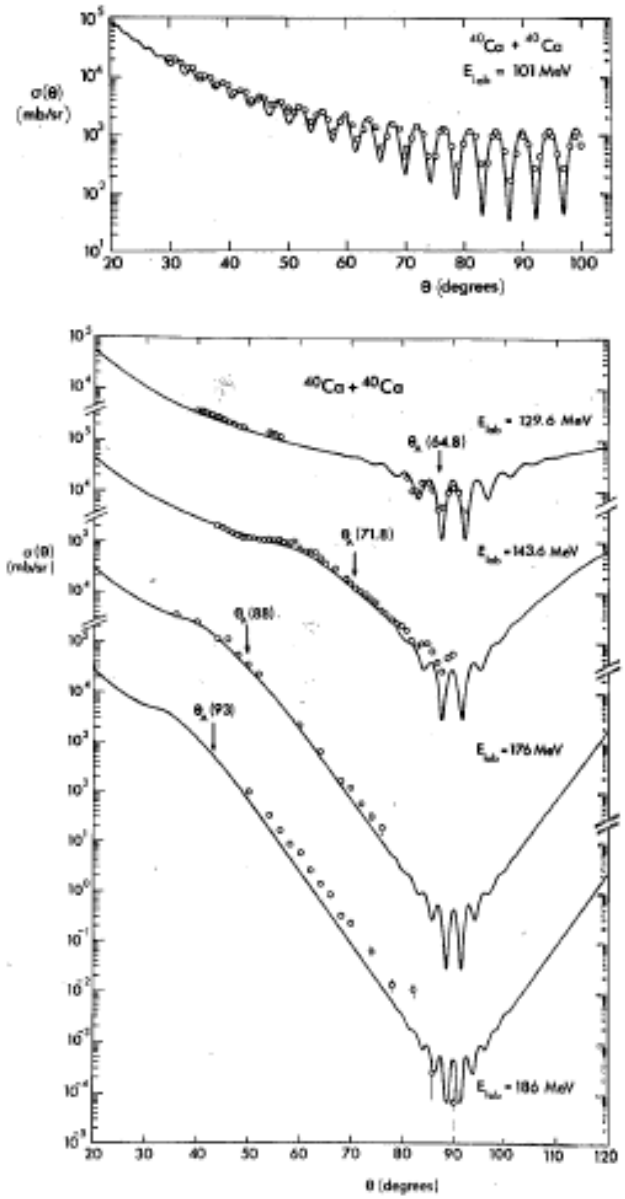

FIG. 11.6. Angular distributions for $^{40}Ca + ^{40}Ca$ elastic scattering at various energies. The curve for 101 MeV is for Mott scattering; those for the other energies were obtained using a parameterized *S*-matrix. (From Fruhn and Rehm 1978.)

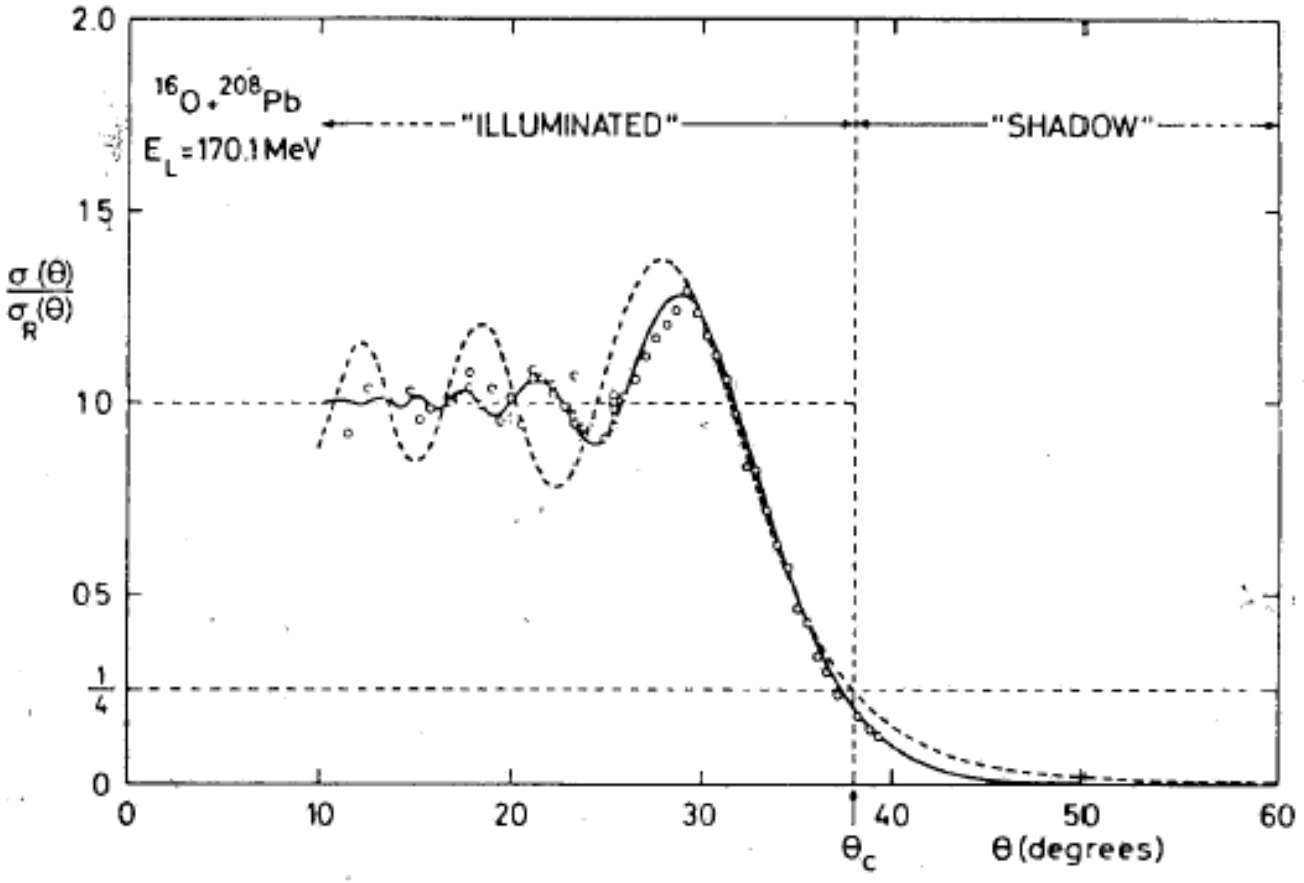

FIG. 11.8. Ratio of elastic cross sections for $^{16}O + ^{208}Pb$ at 170 MeV to the Rutherford cross section. The dashed curve is the simple Fresnel prediction of (11.25), the solid curve was obtained with a parameterized *S*-matrix. (From Frahn 1972.)

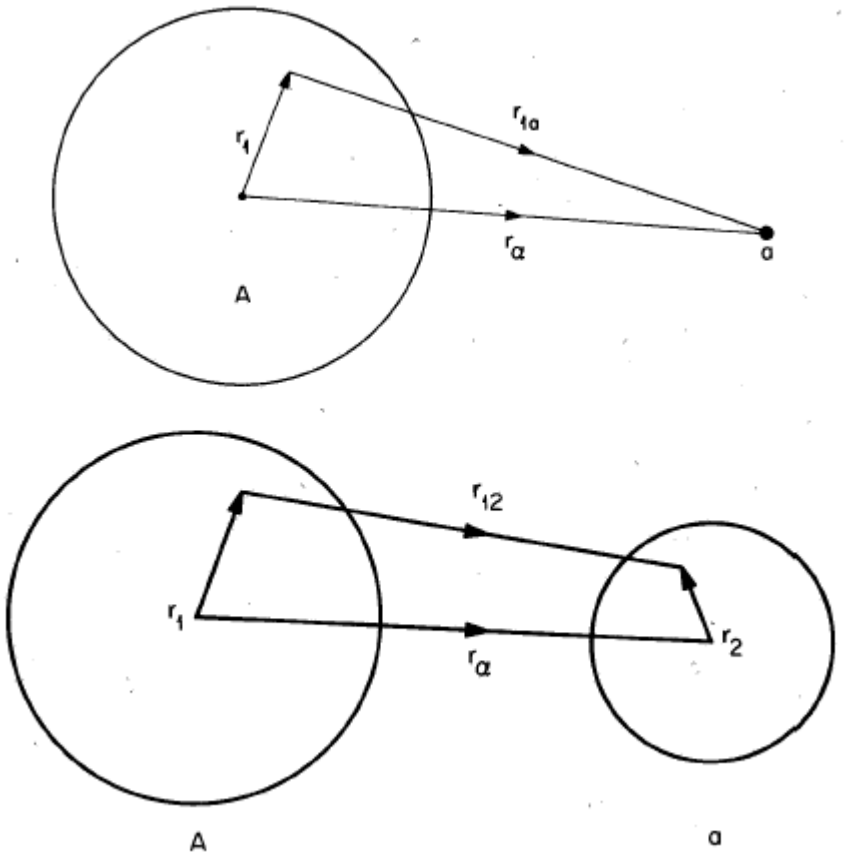

FIG. 12.2. Coordinates used for (a) single-folding, and (b) double-folding.

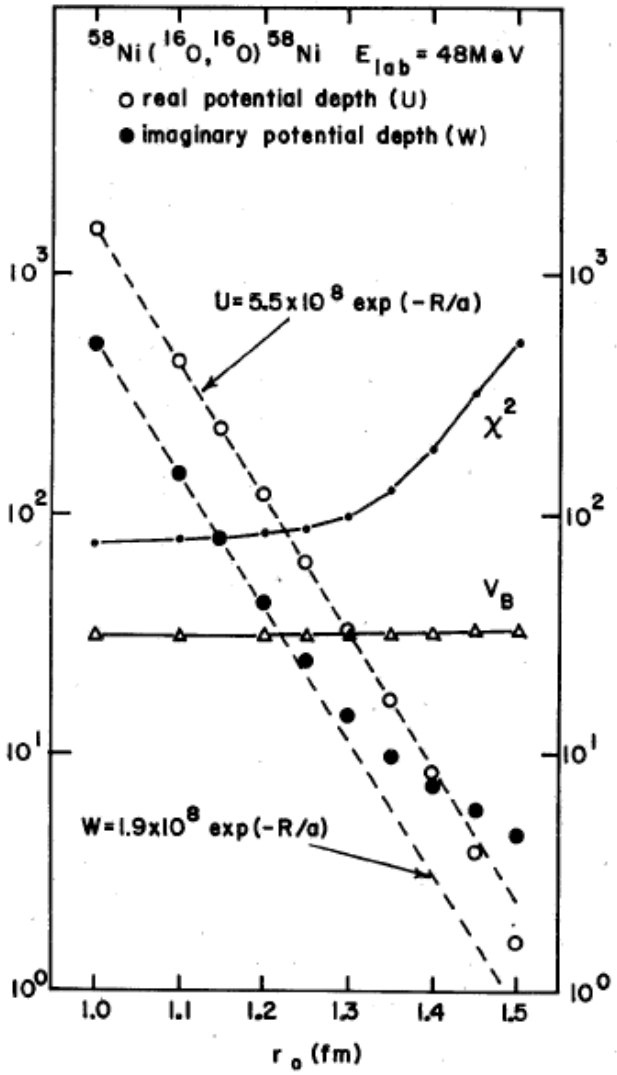

Continuous ambiguities of the Igo type found when Woods-Saxon potential
e $^{16}O + ^{58}Ni$ scattering. Plotted are the optimum values of the real and imag
ınd when the radius parameter r_0 is fixed at various values. The ambiguities
n. The diffuseness was fixed at $a = 0.5$ fm. Also shown is the height V_B of the
'rom West et al. 1975.)

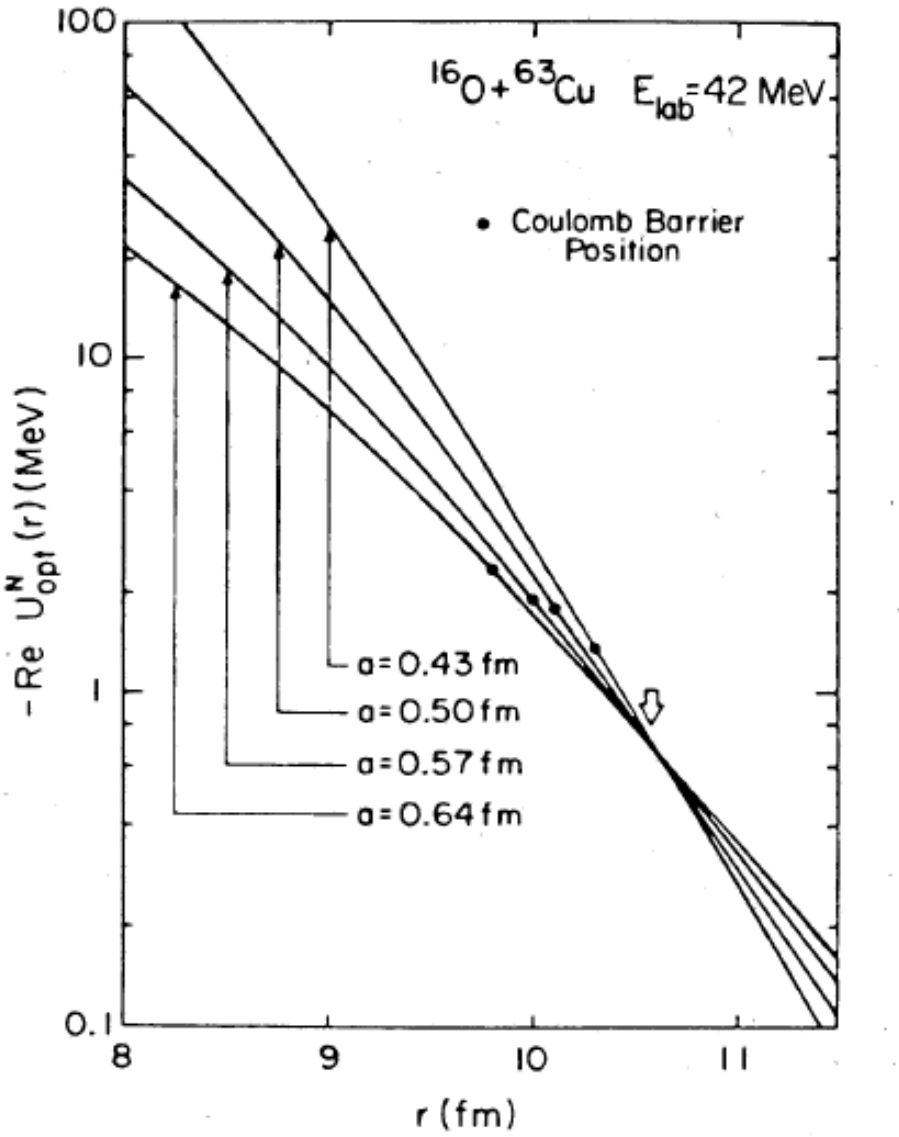

FIG. 12.13. The common intersection near the strong-absorption radius of Woods–Saxon potentials with a series of different surface diffuseness parameters *a* that give equally good fits to the scattering data. (From Wojciechowski et al. 1978.)